European Journal of Organic Chemistry

EurJOC
European Journal of Organic Chemistry

Chemistry Europe
European Chemical Societies Publishing

RESEARCH ARTICLE OPEN ACCESS

Intra- and Intermolecular Glycosylation of D-Idopyranosyl and 6-Deoxy-D-*ido*-heptopyranosyl Donors: Toward the Repeating Unit of *Campylobacter jejuni* HS:4c Capsular Polysaccharide

Maude Cloutier | Nitish Verma | Ilona Douchez | Charles Gauthier

Unité Mixte de Recherche (UMR) INRS-UQAC, Centre Armand-Frappier Santé Biotechnologie, Institut National de la Recherche Scientifique (INRS), Laval and Chicoutimi, Province of Québec, Canada

Correspondence: Charles Gauthier (charles.gauthier@inrs.ca)

Received: 8 September 2025 | **Revised:** 28 October 2025 | **Accepted:** 28 October 2025

Keywords: 6-deoxy-*ido*-heptose | *Campylobacter jejuni* | capsular polysaccharides | disaccharide | intramolecular glycosylation

ABSTRACT

The synthesis of disaccharide mimics of *Campylobacter jejuni* HS:4c capsular polysaccharide, a major pathogen associated with campylobacteriosis, is challenged by the presence of a 1,2-*cis*-β-linked 6-deoxy-D-*ido*-heptopyranoside. Herein, the development of a synthetic route to orthogonally protected D-*ido*-hexo- and 6-deoxy-D-*ido*-heptopyranosyl donors is reported bearing diverse anomeric leaving groups, which represents, to the best of knowledge, the second direct access to 6-deoxy-D-*ido*-heptopyranosides from *ido*-configured precursors. These donors were evaluated in intramolecular aglycon delivery (IAD) and intermolecular glycosylation protocols. While IAD enabled complete β-stereoselectivity with hexosyl donors, it failed with the heptosyl analog. Intermolecular glycosylation provided mixtures of anomers, but the use of a 7-*O*-acetyl-protected heptosyl donor allowed access to the disaccharide in good yield, with chromatographic separation of the α- and β-anomers. Structural analysis revealed unexpected conformational behavior, with the α-disaccharide adopting the $^{1}C_{4}$ chair conformation. This work establishes a foundation for the synthesis of *C. jejuni* HS:4c disaccharides and represents a step toward well-defined sugar-based vaccines candidates against campylobacteriosis.

1 | Introduction

Campylobacter spp. are a major cause of bacterial diarrheal disease and have been classified as a serious threat by the Centers for Disease Control and Prevention in their 2019 Antibiotic Resistance Threats Report [1] and as a high priority pathogen by the World Health Organization [2]. Globally, *Campylobacter* infections are estimated to cause up to 400 million cases of campylobacteriosis annually, with as many as 90% attributed to the encapsulated Gram-negative bacterium *Campylobacter jejuni* [3–5]. Although campylobacteriosis, typically characterized by bloody diarrhea, abdominal pain, headaches, nausea, and fever [6], is generally self-limiting, severe cases may require hospitalization and antibiotic treatment, and can occasionally be fatal. That increasing prevalence of antibiotic resistance in *C. jejuni* further complicates therapeutic management [7–9]. Moreover, *C. jejuni* infection is the leading antecedent factor associated with Guillain-Barré syndrome (GBS), an autoimmune neuropathy [10]. This link arises because the lipooligosaccharides (LOS) in the outer membrane of *C. jejuni* contain β-D-galactoside and α-*N*-acetyl-D-neuraminic acid residues that structurally mimic human gangliosides [11, 12]. As a

Maude Cloutier and Nitish Verma contributed equally to this work.

result, host antibodies generated against these LOS can cross-react with peripheral nerve components, triggering an autoimmune response that leads to GBS.

The significant health burden associated with *C. jejuni* underscores the need for effective prophylactic strategies [13]. In this context, *C. jejuni* capsular polysaccharides (CPS) have emerged as promising targets for oligosaccharide-based vaccine development due to their critical roles as virulence factors and mediators of host–pathogen interactions [14–17]. Notably, glycoconjugate vaccines incorporating CPS from *C. jejuni* HS:4c and HS:23/36 have demonstrated protective efficacy in animal models [18, 19], highlighting their potential for clinical translation.

C. jejuni HS:4c ranks among the ten most prevalent serotypes, accounting for up to 70% of infections in regions including Africa, the Middle East, Southeast Asia, and South America [20–23]. This epidemiological significance has spurred growing interest in the chemical synthesis of its distinctive CPS. The repeating unit of *C. jejuni* HS:4c CPS is a disaccharide composed of a rare 6-deoxy-D-*ido*-heptopyranosyl residue linked to 2-acetamido-2-deoxy-D-glucose (GlcNAc) via a 1,2-*cis*-β glycosidic bond (Figure 1) [20, 24]. The hydroxyl groups at C2 and C7 of the heptose unit are variably substituted with methyl phosphoramidate (MeOPN) groups. Remarkably, MeOPN modifications are present in ≈70% of *C. jejuni* isolates but have not been observed in any other known organism to date [25], suggesting a unique biological role in this pathogen. Evidence indicates that these MeOPN moieties may contribute to host colonization and serum resistance [26, 27], further emphasizing their importance in virulence and vaccine design.

In this context, the synthesis of *C. jejuni* HS:4c CPS mimics has received increasing attention in recent years [28–36]. Key synthetic challenges include the construction of the rare *ido* configuration and the thermodynamically disfavored 1,2-*cis*-β glycosidic linkage. These have been addressed through indirect strategies involving the formation of 1,2-*trans*-β-linked galactosides (Figure 2A) [31, 32] or gulosides (Figure 2B) [35], where neighboring group participation from C2 esters ensures β-selectivity. The resulting intermediates are then epimerized at C2 (from *gulo*) or at both C2 and C3 (from *galacto*) to access the desired *ido* configuration and 1,2-*cis*-β-linkage. In both approaches, the 6-deoxyheptose scaffold is typically established prior to glycosylation, either via homologation of the galactoside precursor or through a C1-to-C5 chain reorganization strategy starting from an allyl α-D-*C*-galactoside.

Although these indirect approaches have proven effective, a direct and stereoselective β-idosylation would represent a significant advance in synthetic efficiency. While we were developing our own approach, Li and coworkers [36] reported a gold(I)-catalyzed protocol for the direct formation of β-D-idopyranosidic

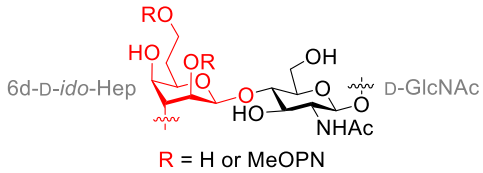

FIGURE 1 | Structure of *C. jejuni* HS:4c capsular polysaccharide repeating unit.

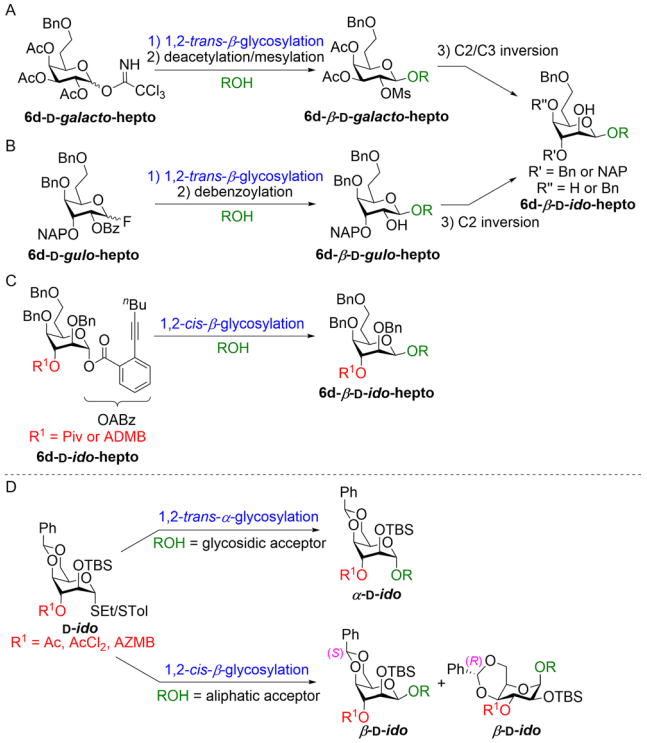

FIGURE 2 | Previous approaches toward the synthesis of 1,2-*cis*-β-linked idopyranosides from (**A**) 6-deoxy-D-*galacto*-hepto [31], (**B**) 6-deoxy-D-*gulo*-hepto [35], (**C**) 6-deoxy-D-*ido*-hepto [36], and (**D**) benzylidene-protected D-*ido*-hexo derivatives (our previous work) [37], Ac: acetyl; $AcCl_2$: dichloroacetyl; ADMB; 4-acetoxy-2,2-dimethylbutanoate; AZMB: 2-(azidomethyl)benzoyl; Bn: benzyl; Ms: mesyl; NAP: 2-naphthylmethyl; OABz: *ortho*-alkynylbenzoyl; Piv: pivaloyl; Ph: phenyl; TBS: *tert*-butyldimethylsilyl; SEt: thioethyl; STol: thiotolyl.

bonds using α-configured 6-deoxy-D-*ido*-heptopyranosyl *ortho*-hexynylbenzoates (OABz) donors, enabling efficient assembly of β-linked oligosaccharides found in *C. jejuni* HS:4c CPS (Figure 2C). Notably, they demonstrated that glycoconjugates bearing the disaccharide repeating unit elicit significant immunogenicity, even in the absence of MeOPN modifications, highlighting its potential as a minimal *O*-antigen mimic for vaccine development.

In our previous work (Figure 2D) [37], we reported a direct β-stereoselective method using benzylidene-protected thioidosyl donors. However, high β-selectivity was observed only with aliphatic alcohols whereas with glycosidic acceptors of lower nucleophilicity, the reaction shifted dramatically toward α-selectivity. Considering these limitations, and the clear need for robust, direct idosylation methods, we report herein an evaluation of D-idopyranosyl and 6-deoxy-D-*ido*-heptopyranosyl donors in both intramolecular aglycon delivery (IAD) and intermolecular glycosylation protocols, toward the construction of the disaccharide repeating unit of *C. jejuni* HS:4c CPS.

2 | Results and Discussion

2.1 | IAD Approach

One of the key challenges in the synthesis of *C. jejuni* HS:4c CPS mimics is the formation of the 1,2-*cis*-β glycosidic linkage

between the idoside unit and the GlcNAc moiety. While 1,2-*trans*-β linkages can be readily achieved via neighboring group participation from a C2 ester [38], the stereoselective construction of 1,2-*cis*-β glycosidic bonds remains a significant challenge [39]. Although several methods have been developed for such transformations, IAD stands out as one of the most reliable strategies for achieving high, if not exclusive, β-stereoselectivity [40, 41]. Originally introduced by Hindsgaul [42], IAD has been widely applied to the stereoselective synthesis of notoriously difficult glycosidic linkages, most notably β-mannosides. The methodology has since been extended to a broad range of 1,2-*cis*-linked sugars [11], including α-glucosides, α-arabinofuranosides, and β-rhamnosides. Significant advances were made by Ito and Ogawa, who developed the *p*-methoxybenzyl (PMB)- [43–45] and 2-naphthylmethyl (NAP)-mediated [46] IAD protocols [47], which offer improved efficiency and stereocontrol. This two-step tethering-glycosylation strategy exploits the stereochemistry at C2 to enforce *cis*-fusion in the transient bridged intermediate. NAP- or PMB-mediated IAD begins with oxidative activation of the NAP or PMB group in the presence of the glycosyl acceptor, leading to the formation of mixed acetals (Figure 3A). Subsequent activation of the anomeric leaving group triggers an intramolecular rearrangement that delivers the aglycon with defined stereochemistry, resulting in the formation of the 1,2-*cis*-glycoside. Given our prior success with NAP-mediated IAD in the synthesis of *Burkholderia pseudomallei* and *Burkholderia mallei* CPS mimics containing 1,2-*cis*-β-linked 6-deoxy-D-*manno*-heptosides [48], we hypothesized that this strategy could be adapted to access the β-linked disaccharide repeating unit of *C. jejuni* HS:4c CPS.

As shown in Figure 3B, disaccharides **1** and **2**, representing the repeating unit of *C. jejuni* HS:4c CPS with or without the MeOPN group, respectively, were selected as synthetic goals. We envisioned that the disaccharide could be synthesized via

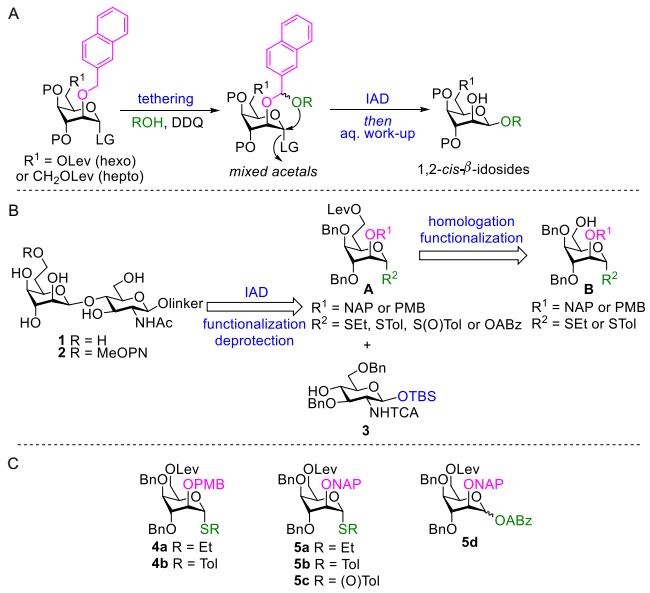

FIGURE 3 | Our proposed strategy for the synthesis of disaccharides **1** and **2**. (**A**) IAD approach; (**B**) retrosynthetic analysis of disaccharides; and (**C**) target model D-*ido*-hexopyranoside donors. Lev: levulinoyl; LG: leaving group; MeOPN: methylphosphoramidate; NHTCA: *N*-trichloroacetamido; P: protecting group; PMB: *para*-methoxybenzyl.

NAP- or PMB-mediated IAD using 6-deoxy-D-*ido*-heptosyl donor **A** and GlcNAc derivative **3** [49]. Donor **A** was designed with orthogonal protection with a 7-*O*-levulinoyl (Lev) group that could be selectively removed to enable installation of the MeOPN moiety at a later stage, if needed. In addition to evaluate both PMB and NAP as tethering groups at C2, we also planned to investigate the influence of the anomeric leaving group. Given the known instability of mixed acetals combined with the general sensitivity of IAD reactions compared to standard intermolecular glycosylations [50], we hypothesized that modifying the leaving group [i.e., SEt, STol, S(O)Tol, and OABz] might enhance both the stability of the mixed acetal intermediates and the reaction kinetics, thereby improving overall yield and reproducibility. We anticipated that donor **A** could be accessed through homologation of a 6-hydroxy-idoside precursor (**B**), bearing either SEt or STol at the anomeric center, followed by conversion to the corresponding OABz or S(O)Tol derivatives.

Expecting that the synthesis of 6-deoxy-D-*ido*-heptosyl donor **A** would be laborious and resource-intensive, we first designed a series of D-*ido*-configured hexopyranosyl donors (**4a**, **4b**, and **5a**–**5d**) as model systems to evaluate the IAD strategy (Figure 3C). We reasoned that the reactivity trends observed with these hexopyranosyl derivatives would closely parallel those bearing heptopyranosyl scaffold, and that the resulting β-disaccharides could be elongated to the heptose scaffold at a later stage of the synthesis. Consistent with our retrosynthetic plan, each model donor bears either a NAP or PMB group at C2 and a range of anomeric leaving groups. Insights gained from these model studies were intended to guide the optimal design of donor **A**, particularly in selecting the most effective combination of C2 tethering group and anomeric leaving group for the final target synthesis.

The synthesis of the model donors is outlined in Scheme 1. Our approach leveraged our previously reported *ido*-configured diols **6a** and **6b** [37], which were prepared in three steps from peracetylated α-D-idopyranoside, accessed via the Paulsen acetoxonium rearrangement of peracetylated β-D-glucopyranose [51]. Benzylation of diols **6a** and **6b** was carried out under phase transfer conditions [52], affording 3-*O*-benzyl derivatives **7a** and **7b**

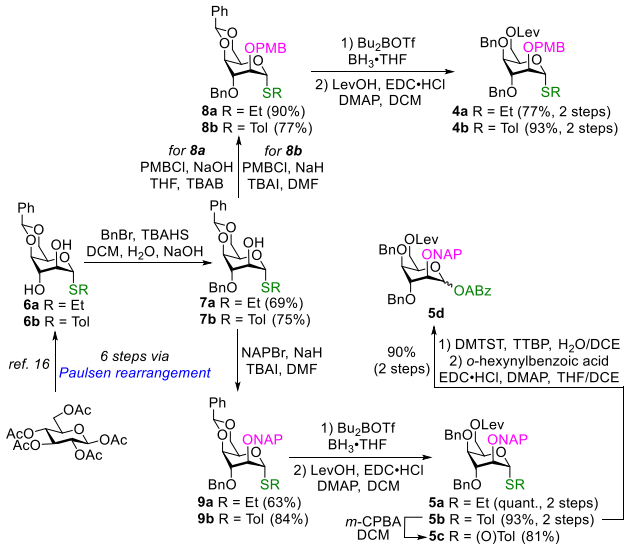

SCHEME 1 | Synthesis of idoside donors **4a**, **4b**, and **5a**–**5d**.

with good regioselectivity. These latter compounds were subsequently subjected to *para*-methoxybenzylation at C2. Notably, when thioethyl-containing intermediate **7a** was treated with NaH, incomplete conversion was observed. However, by employing powdered NaOH in THF [53], the reaction proceeded cleanly and in excellent yield. Next, the benzylidene acetal was regioselectively opened under reductive conditions [54], and the resulting primary alcohol at C6 was levulinoylated to furnish model compounds **4a** and **4b**. In parallel, alcohols **7a** and **7b** were converted into their corresponding 2-*O*-NAP ethers (**9a** and **9b**) using NaH and 2-naphthylmethyl bromide (NAPBr). Subsequent regioselective ring opening of the benzylidene group, followed by levulinoylation at C6, yielded compounds **5a** and **5b** in excellent yields. Donor **5b** was then further derivatized: oxidation with *meta*-chloroperbenzoic acid (*m*-CPBA) provided sulfoxide **5c**, while hemiacetal formation with dimethyl(methylthio)sulfonium trifluoromethanesulfonate (DMTST) followed by esterification with *ortho*-hexynylbenzoic acid [55] furnished OABz donor **5d**.

With the model glycosyl donors in hand, we proceeded to evaluate the IAD reaction under various conditions (Table 1). In all cases, the tethering step between the donor and GlcNAc acceptor **3** was carried out using 2,3-dichloro-5,6-dicyano-1,4-benzoquinone (DDQ) as an oxidant in anhydrous DCM, affording the corresponding mixed acetals. These intermediates were used directly in the subsequent glycosylation step without purification. For the glycosylation, tri-*tert*-butylpyridine (TTBP) was employed as an acid scavenger [41] in the presence of 4 Å molecular sieves to minimize side reactions. Initial studies with thioethyl donor **4a**, bearing a PMB group at C2, revealed that activation with DMTST in 1,2-dichloroethane (DCE) at 40°C delivered desired β-disaccharide **10** in 30% yield as the sole anomer (entry 1), with complete β-selectivity confirmed by nuclear magnetic resonance (NMR) spectroscopy ($^1J_{C1,H1} = 163$ Hz) [56]. Comparable results were obtained when methyl triflate (MeOTf) was used as the promoter (entry 2) or when thiotolyl analog **4b** was activated with DMTST (entry 3). In contrast, conducting the reaction in toluene led to only traces of product formation (entry 4), likely due to poor solubility or inefficient activation under these conditions. Encouraged by these results, we turned to NAP-protected donors **5a**–**5d** in hopes of improving the yield. However, thioethyl donor **5a** proved unstable under oxidative tethering conditions and decomposed during the DDQ-mediated step (entry 5). Fortunately, switching to the more robust thiotolyl donor **5b** allowed successful formation of β-disaccharide **10** in 28% yield (entry 6). Nonetheless, varying the stoichiometry of acceptor **3** (entry 7) or increasing the temperature to 70°C (entry 8) did not lead to any improvement in yield. Attempts to employ sulfoxide **5c** and OABz idonor **5d** under their respective activation protocols failed to yield the desired disaccharide (entries 9–12), suggesting incompatibility of these leaving groups with the IAD sequence.

Although the yields were modest, these results unambiguously demonstrated that the IAD protocol could be successfully applied to *ido*-configured donors **4a**, **4b**, and **5b**, delivering the desired β-disaccharide **10** with complete stereoselectivity. Encouraged by this proof of concept, we decided to advance to the synthesis of the corresponding 6-deoxy-D-*ido*-heptoside donors, aiming to

TABLE 1 | IAD study using idoside donors **4a**, **4b**, and **5a**–**5d**.

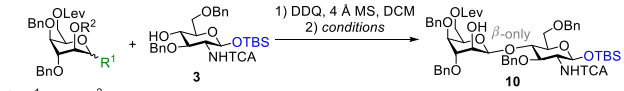

Entry	Donor	Promoter	Solvent	*T* (°C)	*t* (h)	Yield[a] (%)
1	**4a**	DMTST	DCE	40	0.5	30
2	**4a**	MeOTf	DCE	40	19	28
3	**4b**	DMTST	DCE	40	18	27
4	**4b**	DMTST	Tol	40	18	traces
5	**5a**	DMTST	DCE	40	17	N/A[c]
6	**5b**	DMTST	DCE	40	18	28
7[b]	**5b**	DMTST	DCE	40	18	24
8	**5b**	DMTST	DCE	70	18	26
9	**5c**	Tf_2O	DCM	−78 to rt[d]	17	N/A[c]
10	**5c**	Tf_2O	DCM	−78 to −58	1	traces
11	**5d**	NIS/TMSOTf	DCE	0 to rt	4	N/A[c]
12	**5d**	PPh_3AuCl/AgOTf	DCM	−40 to 0	2	N/A[c]

[a]Isolated yield.
[b]1.0 equiv. of acceptor instead of the usual 1.2 equiv.
[c]Decomposition. The reaction was performed in the presence of TTBT and 4 Å MS.
[d]Room temperature (rt).

evaluate whether the IAD strategy could be extended to the more biologically relevant heptopyranosyl system and to further optimize the glycosylation efficiency.

A major hurdle in this endeavor lies in the homologation of hexo- to heptopyranosides while preserving the desired $^4C_1$ conformation. Indeed, Hevey and Ling [30] reported an attempt to elongate an *ido*-configured β-hexopyranoside via a three-step sequence: (1) oxidation of the C6 alcohol; (2) Wittig olefination; and (3) hydroboration-oxidation of the terminal alkene. However, when methyltriphenylphosphonium ylide was employed, the intermediate alkene predominantly adopted the $^1C_4$ conformation instead of the native $^4C_1$ chair. This conformational inversion was attributed to the loss of stabilizing intramolecular hydrogen bonds upon oxidation of the C6 hydroxyl group [30], which resulted in axial orientation of the C5-C6 alkene and increased steric hindrance at the terminal carbon, ultimately leading to failure in the hydroboration step. To circumvent this issue, we hypothesized that employing a methoxymethyl (MOM)-Wittig reaction after oxidation would generate an enol ether intermediate, thereby preserving the electronic and steric environment that favors the $^4C_1$ conformation. The resulting enol ether could then be hydrolyzed under mild acidic conditions to yield the corresponding aldehyde at C7, followed by reduction to install the 6-deoxy functionality, thus completing the homologation sequence.

This homologation strategy was first attempted on the 6-hydroxy thiotolyl idoside bearing a 2-*O*-NAP group. While oxidation of the C6 alcohol under Parikh-Doering conditions [57] proceeded cleanly to yield the corresponding aldehyde, the subsequent MOM-Wittig olefination predominantly delivered the α,β-unsaturated aldehyde via base-mediated elimination of H5 and the adjacent 4-*O*-benzyl-protected oxygen (a 1,2-*trans*-diaxial arrangement). This side reaction persisted even when less hindered ylides, such as methyltriphenylphosphorane, were employed. Although reaction conditions were varied (i.e., switching from THF to toluene as solvent and increasing the temperature from −78 to 0°C), elimination remained the dominant pathway. We hypothesize that this undesired reactivity is exacerbated by the steric bulk and conformation rigidity of the axial 2-*O*-NAP group, which may hinder approach of the ylide and promote deprotonation at C5. Given these persistent challenges, we decided to discontinue studies on the NAP-protected series and shift our focus to the PMB-protected analogs. The corresponding 6-hydroxy thioethyl idoside was also found to be highly unstable under the oxidative conditions and rapidly decomposed, prompting its exclusion from further investigation.

We therefore focused on the remaining viable candidate: the 6-hydroxy thiotolyl idoside bearing a 2-*O*-PMB group. As shown in Scheme 2, regioselective opening of the benzylidene acetal in compound **8b** was achieved using dibutylboron triflate (Bu_2BOTf) affording alcohol **11**. This was oxidized under Parikh-Doering conditions to the aldehyde, which was immediately subjected to MOM-Wittig olefination using potassium hexamethyldisilazide (KHMDS) in a toluene/THF mixture at room temperature. Notably, the use of stronger bases (*n*BuLi, *t*BuOK) or more polar solvents (THF, DMF), as well as lower reaction temperatures (0, −40, and −78°C) favored elimination and led to the formation of the α,β-unsaturated aldehyde, consistent with observations from the NAP series. The desired enol ether was then hydrolyzed under mild acidic conditions to yield the C7 aldehyde, which was reduced with $NaBH_4$ to afford alcool **12**.

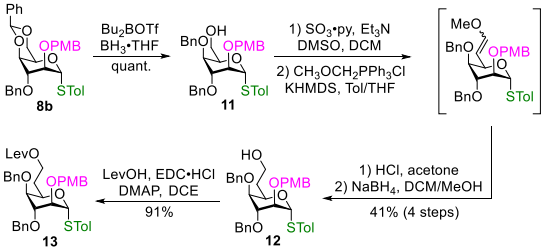

SCHEME 2 | Synthesis of heptoside derivative **13** through homologation.

Importantly, this four-step sequence was optimized to proceed without chromatographic purification of intermediates, significantly improving efficiency. The successful installation of the 6-deoxy-heptose framework was confirmed by ^{1}H and COSY NMR analysis, which revealed two distinct methylene signals for H-6a and H-6b at 2.10 and 1.64 ppm, respectively, each coupled to the signals at 3.64 ppm assigned to H-7a and H-7b. Finally, the primary alcohol at C7 was levulinoylated to furnish target donor **13**.

With a reproducible route to heptosyl donor **13** established, we proceeded to evaluate the IAD coupling with GlcNAc acceptor **3** under previously optimized conditions (Scheme 3). Despite multiple attempts, including varying promoters (DMTST, MeOTf, etc.), temperatures, concentrations, and the nature of molecular sieves, no disaccharide product was observed. Instead, significant decomposition of the donor and acceptor was consistently detected, suggesting instability of the mixed acetal intermediate or inefficient activation under the employed conditions.

2.2 | Intermolecular Glycosylation Approach

Anticipating potential limitations in the IAD approach, we pursued intermolecular glycosylation methods in parallel. Given that 2-*O*-NAP-protected model donors **5b**, **5c**, and **5d** were available in multigram quantities, we aimed to evaluate their reactivity under various activation conditions in the hope of achieving β-stereoselective coupling with GlcNAc acceptor **3** (Table 2). Initial attempts using thiotolyl donor **5b** under DMTST promotion failed to yield any detectable glycosylation product (entry 1). However, when α-sulfoxide donor **5c** was activated with triflic anhydride (Tf_2O) at low temperature, disaccharide **19** was obtained in good yield as a 1.0:1.2 α/β mixture that could not be separated by standard chromatography (entry 2). Encouraged by recent reports from Yu's [58, 59] and Li's [60, 61], who demonstrated that gold(I)-catalyzed activation of α-configured OABz donors generates a glycosyloxy isocoumarin intermediate that undergoes S_N2-type displacement to afford β-linked glycosides with high stereoselectivity, we investigated the use of OABz donor **5d** for the synthesis of the β-linked disaccharide. Although pure α-anomeric **5d** was not accessible due to anomeric epimerization

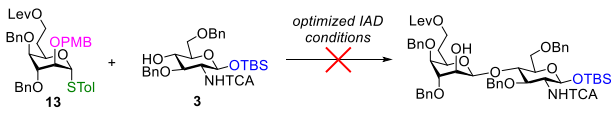

SCHEME 3 | Unsuccessful IAD attempts using heptoside **13**.

TABLE 2 | Intermolecular glycosylation study with model idoside donors.

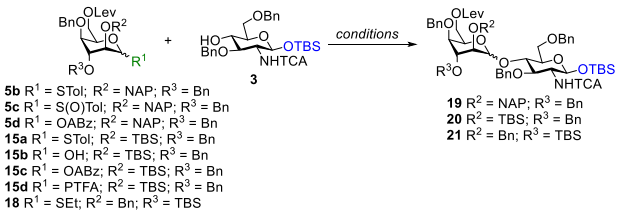

Entry	Donor	Promoter	Solvent	*T* (°C)	*t* (h)	Yield[a] (%) (α/β)
1	**5b**	DMTST	DCE	rt	1	N/A
2	**5c**	Tf_2O/TTBP	DCM	−78 to −60	1.5	70[b] (1:1.2)
3	**5d**	NIS/TMSOTf	DCE	0 to rt	2	71[b] (2.2:1)
4	**5d**	PPh_3AuCl/AgOTf	DCM	−40	1	83[b] (1.5:1)
5	**5d**	PPh_3AuCl/AgOTf	DCM/ACN	−40 to rt	3	N/A[c]
6	**15c**	NIS/TMSOTf	DCE	−10 to rt	1	N/A[d]
7	**15c**	PPh_3AuCl/AgOTf	DCM	−40 to rt	21	N/A[d]
8	**15a**	NIS/TMSOTf	DCE	−10 to rt	1	55 (3.7:1)
9	**15a**	NIS/TMSOTf	DCM/ACN	−40	1	59 (1.7:1)
10	**15b**	Ph_3PO, $(COCl)_2$, LiI, iPr_2NEt	$CHCl_3$	rt to 45	24	N/A[c]
11	**15b**	KHMDS/Ts_2O	THF	−78 to rt	21	N/A[c]
12	**15d**	TMSOTf	DCM/ACN	−60 to rt	1	20 (1:0)
13	**15d**	$FeCl_3$	DCM/ACN	−60 to rt	1	9[b] (2:1)
14	**18**	NIS/TMSOTf	DCM/ACN	−40	1	12 (1:0)

[a]Isolated yield.
[b]Contaminated with unseparable impurity.
[c]Donor decomposed.
[d]No reaction.

during synthesis, the anomeric mixture was subjected to activation with NIS/TMSOTf. This afforded disaccharide **19** as an α/β mixture with a slight preference for the α-anomer (entry 3). Similar results were observed when PPh_3AuCl/AgOTf was used as the promoter system in DCM (entry 4). Switching the solvent to a mixture of DCM/ACN, however, led to complete decomposition of the donor (entry 5). Not only did these conditions fail to deliver significant β-selectivity, but the resulting disaccharides were consistently contaminated with an inseparable impurity, regardless of the leaving group [STol, S(O)Tol, or OABz]. While the α/β ratio could be estimated by undecoupled HSQC NMR analysis, and product formation was confirmed by high resolution mass spectrometry (*m*/*z* 1215.4370, $[M + NH_4]^+$), full structural characterization was precluded due to the persistent presence of impurity. This limitation prompted us to explore alternative idosyl donor systems in search of improved reactivity and cleaner reaction profiles.

In their development of a β-mannosylation protocol, Li and colleagues [62] observed that installing a 2-*O*-silyl group on a 4,6-*O*-benzylidene-protected mannosyl OABz donor significantly enhanced β-stereoselectivity. This finding served as the foundation for their recent strategy toward the synthesis of β-1, 6-linked oligomannosides [61]. Similarly, Yu et al. [59] demonstrated that 2-*O*-TBS-protected mannosyl donors exhibited improved β-selectivity in glycosylation reactions. Inspired by these reports, we hypothesized that introducing a 2-*O*-TBS group on an idosyl OABz donor might similarly promote β-selective glycosylation. Although the bulky TBS group could impose steric hindrance on the α-face of the sugar, we reasoned that its electron-donating character might increase the nucleophilicity of the endocyclic oxygen, thereby stabilizing the oxocarbenium ion intermediate and favoring attack from the β-face via a more compact, kinetically controlled transition state. Furthermore, we anticipated that conducting the reaction at low temperature might further enhance kinetic β-selectivity.

As shown in Scheme 4A, the synthesis of the target donor began with alcohol **7b**, which was silylated at C2 using *tert*-butyldimethylsilyl triflate (TBSOTf) to afford compound **14**. Subsequent regioselective opening of the benzylidene acetal, followed by levulinoylation at C6, yielded thiotolyl donor **15a**. This was then activated with *N*-bromosuccinimide (NBS) to generate the hemiacetal, which was esterified with *ortho*-hexynylbenzoic acid to furnish the OABz donor **15c** as an α/β anomeric mixture. Despite successful preparation of compound **15c**, attempts to glycosylate GlcNAc acceptor **3** under either NIS/TMSOTf or PPh_3AuCl/AgOTf promotion (Table 2, entries 6 and 7, respectively) failed to yield the desired disaccharide. No product formation was observed and only decomposition of the donor and acceptor was detected under both sets of conditions.

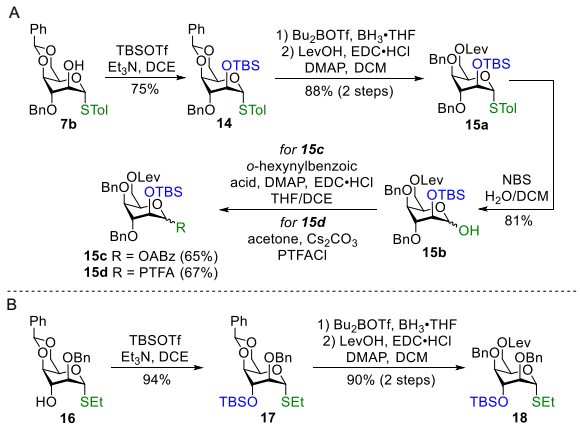

SCHEME 4 | Synthesis of (**A**) 2-*O*-TBS and (**B**) 3-*O*-TBS donors **15a–15d** and **18**.

Considering the unsuccessful results with 2-*O*-TBS-protected OABz donor **15c**, we turned our attention to other donor types: thiotolyl **15a**, hemiacetal **15b**, and *N*-phenyltrifluoroacetimidate (PTFA) **15d** (Scheme 4A). Concurrently, we pursued the synthesis of 3-*O*-silylated thioethyl donor **18** (Scheme 4B) using alcohol **16**, a byproduct isolated during the 3-*O*-regioselective benzylation step in the early stages of our synthetic sequence (see Scheme 1). We hypothesized that placing a bulky TBS group at C3, on the α-face of the pyranose ring, might sterically shield this face and thereby favor nucleophilic attack from the β-face, leading to the formation of the β-glycoside via an S_N2-like displacement or through conformational steering of the oxocarbenium ion.

With this expanded set of donors in hand, we resumed our intermolecular glycosylation studies (Table 2). Activation of thiotolyl donor **15a** with NIS/TMSOTf in DCE yielded the corresponding disaccharide with slight α-selectivity (entry 8). Although switching to a DCM/ACN mixture improved the α/β ratio, the α-anomer remained the major product (entry 9). Encouraged by the work of McGarrigle and coworkers, who developed a β-selective manno- and rhamnosylation protocol using hemiacetal via a one-pot sequence involving chlorination, iodination, and glycosylation [63], we applied their optimized conditions to hemiacetal **15b**. However, no glycosylation product was observed under these conditions (entry 10). Similarly, an alternative strategy based on the formation of an α-glycosyl tosylate intermediate, previously employed by Bennett and colleagues for the stereospecific synthesis of β-linked 2-deoxy sugars [64], proved ineffective in our system (entry 11). TMSOTf-mediated activation of PTFA donor **15d** in DCM/ACN proceeded sluggishly and with complete α-selectivity (entry 12). When $FeCl_3$ was used as a milder promoter, the anomeric ratio improved slightly toward the β-anomer, but the overall yield remained low (entry 13). Finally, contrary to our expectations, glycosylation using 3-*O*-TBS donor **18** afforded only the α-linked disaccharide **21**, with no detectable β-product (entry 14). These results indicate that steric shielding at C3 is insufficient to override the inherent α-directing effects in idosyl glycosylations under the conditions explored.

Although our various attempts to achieve efficient and β-selective intermolecular glycosylation with hexopyranosyl-based donors met with limited success, we were nonetheless keen to evaluate the reactivity of the fully elaborated 6-deoxy-D-*ido*-heptopyranosyl donor system. With donor **12** available in sufficient quantities, we turned to its protected derivative **13** (7-*O*-levulinoylated) for glycosylation trials under conditions informed by earlier screening (Table 3). Based on the improved anomeric ratio observed in entry 8 of Table 2 (NIS/TMSOTf, DCM/ACN, −40°C), we selected this protocol as a starting point. Coupling of donor **13** with GlcNAc acceptor **3** under these conditions proceeded to completion, affording an anomeric mixture of disaccharides **24α** and **24β** in a 2:1 ratio, with the α-anomer predominating (entry 1). Encouragingly, the two anomers could be separated by flash chromatography, a notable improvement over previous systems where inseparable anomeric mixtures were obtained. To improve the β-selectivity, we explored lower temperatures and alternative solvents, including propionitrile, which has been reported to favor β-pathways in certain glycosylations [65]. However, these modifications failed to shift the stereoselectivity in favor of the β-anomer (entry 2). Although both disaccharides were isolable, we encountered a persistent issue: the β-linked product (**24β**) coeluted with a significant impurity that resisted all attempts at separation, including multiple chromatographic systems and solvent gradients. As a result, pure **24β** could not be isolated. Nevertheless, its formation was unambiguously confirmed by high-resolution mass spectrometry (HRMS)

TABLE 3 | Intermolecular glycosylation study with 6-deoxy-D-*ido*-heptopyranosyl donors 13, 22, and 23.

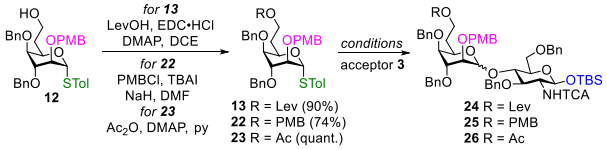

Entry	Donor	Promoter	Solvent	*T* (°C)	*t* (h)	Yield[a] (%) (α/β)
1	**13**	NIS/TMSOTf	DCM/ACN	−40	1	85[b] (2:1)
2	**13**	NIS/TMSOTf	propionitrile	−60 to −40	1	20[b] (2.5:1)
3	**22**	NIS/TMSOTf	DCM/ACN	−40	1	traces
4	**23**	NIS/TMSOTf	DCM/ACN	−40	1	87 (1.7:1)

[a]Isolated yield.
[b]β-anomer contaminated with unknown impurity.

(m/z $[M + NH_4]^+$ calcd for $C_{62}H_{80}[^{35}Cl]_3N_2O_{14}Si$ 1209.4439; found 1209.4399). It is worth mentioning that a sulfoxide derivative was also prepared from glycosyl donor **13**. However, its intrinsic instability under the glycosylation conditions (Tf_2O/TTBP) precluded further evaluation.

The poor β-stereoselectivity observed in the glycosylation with donor **13**, combined with the persistent challenges in isolating the disaccharide **24β** free from impurities, prompted us to explore alternative 6-deoxy-D-*ido*-heptopyranosyl donors. We hypothesized that the preference for the α-anomer might arise from remote anchimeric assistance by the 7-*O*-Lev group [66]. Although C7 is distal to the anomeric center, the flexibility of the heptose side chain could allow transient participation of the ester carbonyl in stabilizing an oxocarbenium ion intermediate, potentially favoring α-attack through conformational bias or ion pairing effects. To test this hypothesis, we prepared donor **22**, in which the Lev group was replaced with a PMB ether, a nonparticipating, yet easily removable protecting group. However, under standard activation conditions (NIS/TMSOTf, DCM/ACN, −40°C), the glycosylation proceeded poorly, yielding only trace amounts of coupling product (entry 3). HRMS analysis confirmed the presence of the desired disaccharide (m/z 1231.4600 ($[M + NH_4]^+$), but the low yield precluded isolation and full characterization. Given this lack of reactivity, we turned to 7-*O*-acetyl derivative **23**, reasoning that the acetyl group, while still an ester, might exhibit weaker or less disruptive neighboring group participation, compared to the Lev moiety. Encouragingly, activation of donor **23** with NIS/TMSOTf in DCM/ACN at −40°C delivered disaccharide **26** in good yield and with improved stereoselectivity (ratio α/β = 1.7:1.0, entry 4). Importantly, both anomers were cleanly separated by flash chromatography, allowing access to each pure stereoisomer, marking the first time in this study that the β-linked heptoside could be isolated in analytically pure form.

Due to the axial orientation of the C2 substituent in D-*ido*-pyranosides, determination of the anomeric configuration by $^3J_{H1,H2}$ coupling constants is typically unreliable. In the $^4C_1$ conformation, both α- and β-anomers exhibit small $^3J_{H1,H2}$ values because H1 and H2 are nearly perpendicular (dihedral angle ≈90°) precluding meaningful stereochemical assignment based on this parameter alone. A more reliable diagnostic is the $^1J_{C1,H1}$ coupling constant: β-linked glycosides (with an axially oriented H1) typically display values around 160 Hz, whereas α-anomers (with an equatorially oriented H1) show values near 170 Hz [32]. For disaccharide **26**, we anticipated a $^1J_{C1,H1}$ of ≈160 Hz for the β-anomer and 170 Hz for the α-anomer. Indeed, the β-anomer was readily assigned by its $^1J_{C1,H1}$ of 162 Hz, consistent with an axial H1 and β-oriented anomeric configuration. However, analysis of the second anomer gave a less definitive result with a $^1J_{C1,H1}$ of 165 Hz, which is intermediate between typical values for α- and β-linked idosides. Further ^1H NMR analysis revealed that the protons H-1, H-2, and H-3 of the *ido*-heptopyranoside unit in this compound exhibited unusually large coupling constants, most notably a $^3J_{H1,H2}$ of 7.1 Hz. This value is diagnostic of a *trans*-diaxial relationship, which can only occur if the pyranose ring adopts the $^1C_4$ conformation (Figure 4). Based on this evidence, the anomeric configuration was confidently assigned as α, with H1 axial in the inverted chair. The same conformational behavior was observed for disaccharide **24α**. In contrast, the ido unit in compound **26β** displayed small interproton coupling constants, consistent with a $^4C_1$ conformation and typical

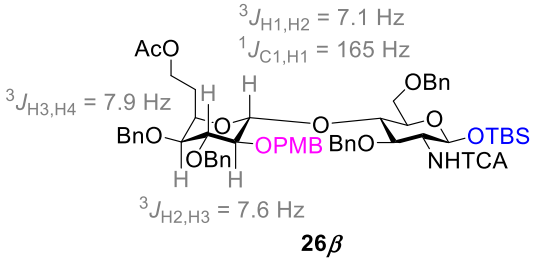

FIGURE 4 | Key NMR coupling constants observed in disaccharide **26α** suggesting a $^1C_4$ conformation for the *ido*-heptopyranose ring.

dihedral angles found in idopyranosides. While this result is initially surprising, given that α-idosides are traditionally expected to be stabilized in the $^4C_1$ conformation by the anomeric effect [16], it further underscores the exceptional conformational flexibility of idose-containing systems. The ability of the α-anomer to adopt the $^1C_4$ chair under glycosidic conditions highlights the delicate balance of stereoelectronic and steric factors governing idoside behavior, reinforcing their reputation as uniquely dynamic and unpredictable sugars.

3 | Conclusion

In summary, we report our progress toward the synthesis of disaccharide mimics of *C. jejuni* HS:4c CPS, one of the predominant serotypes associated with campylobacteriosis worldwide. We have developed a synthetic route to access orthogonally protected D-*ido*-hexopyranosyl and 6-deoxy-D-*ido*-heptopyranosyl donors bearing diverse anomeric leaving groups. To the best of our knowledge, this represents the second synthetic approach enabling direct access to 6-deoxy-D-*ido*-heptopyranosides from *ido*-configured precursors. These donors were employed in an extensive glycosylation study encompassing both IAD and intermolecular protocols. While IAD with *ido*-hexopyranosyl donors proceeded with complete β-stereoselectivity, the method failed when applied to the 6-deoxy-D-*ido*-heptopyranosyl donor. In intermolecular glycosylations, high β-selectivity was not achieved, however, the use of 7-*O*-acetyl donor **23** afforded the disaccharide in good yield, with the α- and β-anomers being chromatographically separable. We anticipate that further optimization of the reaction conditions may enhance β-stereoselectivity. Further work will focus on the scale-up synthesis of β-disaccharide **26**, followed by orthogonal deprotection and functionalization to access target compounds **1** and **2**. Late-stage homologation of the β-disaccharides containing the idohexose scaffold, obtained through IAD, could also be a potential avenue. The target compounds could then be conjugated to a carrier protein for subsequent immunogenicity studies. Altogether, this work represents a significant step forward in the synthetic access to *C. jejuni* Hs:4c oligosaccharides from functionalized D-idose precursors, laying a foundation for the development of well-defined glycoconjugate vaccine candidates against campylobacteriosis.

Acknowledgments

This work was supported by funds from a Natural Sciences and Engineering Research Council of Canada (NSERC) Discovery grant

(RGPIN-2022−04515, to C.G.) and a PTR (Programmes Transversaux de Recherche) grant (PTR 380−20, to C.G.) from Institut Pasteur, Paris. C.G. was also supported by a Fonds de recherche du Québec – Santé (FRQS) Research Scholars Senior Career Award. M.C. thanks NSERC Vanier and Fonds de recherche du Québec – Nature et technologies (FRQNT) for Ph.D. scholarships. N.V. thanks the Swine and Poultry Infectious Diseases Research Center (CRIPA) for a postdoctoral fellowship.

Funding

This work was supported by the Natural Sciences and Engineering Research Council of Canada (RGPIN-2022−04515, to C.G), Programmes Transversaux de Recherche (PTR 380−20, to C.G).

Conflicts of Interest

The authors declare no conflicts of interest.

Data Availability Statement

The data that support the findings of this study are available from the corresponding author upon reasonable request.

References

1. Centers for Disease Control and Prevention (US), "*Antibiotic Resistance Threats in the United States*," (Atlanta: Department of Health and Human Services, CDC, 2019).

2. *World Health Organization, Bacterial Priority Pathogens List, 2024: Bacterial Pathogens of Public Health Importance to Guide Research*, (Geneva: Development and Strategies to Prevent and Control Antimicrobial Resistance, 2024).

3. M. B. Batz, S. Hoffmann, and J. G. J. Morris, "Ranking the Disease Burden of 14 Pathogens in Food Sources in the United States Using Attribution Data from Outbreak Investigations and Expert Elicitation," *Journal of Food Protection* 75 (2012): 1278–1291.

4. E. K. Jagusztyn-Krynicka, P. Łaniewski, and A. Wyszyńska, "Update on *Campylobacter Jejuni* Vaccine Development for Preventing Human Campylobacteriosis," *Expert Review of Vaccines* 8 (2009): 625–645.

5. M. O'Ryan, R. Vidal, F. del Canto, J. C. Salazar, and D. Montero, "Vaccines for viral and Bacterial Pathogens Causing Acute Gastroenteritis: Part II: Vaccines for *Shigella*, *Salmonella*, enterotoxigenic *E. coli* (ETEC), Enterohemorragic *E. coli* (EHEC) and *Campylobacter jejuni*," *Human Vaccines Immunotherapeutics* 11 (2015): 601–619.

6. I. Hansson, M. Sandberg, I. Habib, R. Lowman, and E. O. Engvall, "Knowledge gaps in Control of *Campylobacter* for Prevention of Campylobacteriosis," *Transboundary and Emerging Diseases* 65, 2018): 30–48.

7. J. C. Lindow, F. Poly, D. R. Tribble, et al., "Caught in the act: in vivo Development of Macrolide Resistance to *Campylobacter jejuni* Infection," *Journal of Clinical. Microbiology* 48 (2010): 3012–3015.

8. S. Kittl, P. Kuhnert, H. Hächler, and B. M. Korczak, "Comparison of Genotypes and Antibiotic Resistance Of *Campylobacter Jejuni* Isolated From Humans and Slaughtered Chickens in Switzerland," *Journal of Applied Microbiology* 110 (2011): 513–520.

9. S. Zhao, S. R. Young, E. Tong, et al., "Antimicrobial Resistance of *Campylobacter* Isolates from Retail Meat in the United States between 2002 and 2007," *Applied and Environmental Microbiology* 76 (2010): 7949–7956.

10. S. Kuwabara and N. Yuki, "Axonal Guillain-Barré Syndrome: Concepts and Controversies," *The Lancet Neurology.* 12 (2013): 1180–1188.

11. A. Moran, B. Appelmelk, and G. Aspinall, "Molecular Mimicry of Host Structures by Lipopolysaccharides of *Campylobacter* and *Helicobacter* spp.: Implications in Pathogenesis," *Journal of Endotoxin Research* 3 (1996): 521–531.

12. A. Moran and D. O'Malley, "Potential Role of Lipopolysaccharides of *Campylobacter jejuni* in the development of Guillain-Barré syndrome," *Journal of Endotoxin Research*, 2 (1995): 233–235.

13. M. Cloutier and C. Gauthier, "Progress Toward the Development of Glycan-Based Vaccines Against Campylobacteriosis," *ACS Infectious Diseases* 7 (2020): 969–986.

14. D. J. Bacon, C. M. Szymanski, D. H. Burr, R. P. Silver, R. A. Alm, and P. Guerry, "A Phase-Variable Capsule is Involved in Virulence of *Campylobacter Jejuni* 81-176," *Molecular Microbiology* 40 (2001): 769–777.

15. B. M. Bachtiar, P. J. Coloe, and B. N. Fry, "Knockout mutagenesis of the kpsE gene of *Campylobacter jejuni* 81116 and its involvement in bacterium-host interactions," *FEMS Immunology and Medical Microbiology* 49 (2007): 149–154.

16. N. Corcionivoschi, M. Clyne, A. Lyons, et al., "*Campylobacter Jejuni* Cocultured with Epithelial Cells Reduces Surface Capsular Polysaccharide Expression," *Infection and Immunity* 77 (2009): 1959–1967.

17. P. Guerry and C. M. Szymanski, "*Campylobacter* Sugars Sticking out," *Trends in Microbiology* 16 (2008): 428–435.

18. M. A. Monteiro, S. Baqar, E. R. Hall, et al., "Capsule Polysaccharide Conjugate Vaccine Against Diarrheal Disease Caused by *Campylobacter Jejuni*," *Infection and Immunity* 77 (2009): 1128–1136.

19. F. R. Jones, S. Baqar, A. Gozalo, et al.,"New World Monkey *Aotus nancymae* as a Model for *Campylobacter Jejuni* Infection and Immunity," *Infection and Immunity* 74 (2006): 790–793.

20. F. Poly, O. Serichantalergs, J. Kuroiwa, et al., "Updated *Campylobacter Jejuni* Capsule PCR Multiplex Typing System and its Application to Clinical Isolates from South and Southeast Asia," *PLoS ONE* 10 (2015): e0144349.

21. M. A. Monteiro, A. Noll, R. M. Laird, et al., "Campylobacter Jejuni Capsule Polysaccharide Conjugate Vaccine," in Carbohydrate-Based Vaccines: From Concept to Clinic (ACS Publications, 2018), 249–271.

22. R. Sainato, A. ElGendy, F. Poly, et al., "Epidemiology of *Campylobacter* Infections Among Children in Egypt," *The American Journal of Tropical Medicine and Hygiene* 98 (2017): 581.

23. J. D. Rojas, N. D. Reynolds, B. L. Pike, et al., "Distribution of Capsular Types of *Campylobacter Jejuni* Isolates from Symptomatic A[1]nd Asymptomatic Children in Peru," *The American Journal of Tropical Medicine and Hygiene* 101 (2019): 541.

24. Y. H. Chen, F. Poly, Z. Pakulski, P. Guerry, and M. A. Monteiro, "The Chemical Structure and Genetic Locus of *Campylobacter Jejuni* Cg8486 (Serotype Hs:4) Capsular Polysaccharide: The Identification of 6-Deoxy-D-Ido-Heptopyranose," *Carbohydrate Research* 343 (2008): 1034–1040.

25. D. J. McNally, M. P. Lamoureux, A. V. Karlyshev, et al., "Commonality and Biosynthesis of The O-Methyl Phosphoramidate Capsule Modification in *Campylobacter Jejuni*," *The Journal of Biological Chemistry* 282 (2007): 28566–28576.

26. A. C. Maue, K. L. Mohawk, D. K. Giles, et al., "The Polysaccharide Capsule of *Campylobacter Jejuni* Modulates the Host Immune Response," *Infection and Immunity* 81 (2013): 665–672.

27. L. B. van Alphen, C. Q. Wenzel, M. R. Richards, et al., "Biological Roles of the O-Methyl Phosphoramidate Capsule Modification in *Campylobacter jejuni*," *PLoS ONE* 9 (2014): e87051.

28. R. Hevey, X. Chen, and C. C. Ling, "Role of the 4,6-O-Acetal in the Regio- and Stereoselective Conversion of 2,3-di-O-Sulfonyl-β-D-Galactopyranosides to D-Idopyranosides," *Carbohydrate Research* 376 (2013): 37–48.

29. R. Hevey and C.-C. Ling, "Evidence of cation-Coordination Involvement in Directing the Regioselective Di-Inversion Reaction of Vicinal Di-Sulfonate Esters," *Organic & Biomolecular Chemistry* 11 (2021): 1088–1895.

30. R. Hevey and C.-C. Ling, "Studies on the 6-Homologation of β-D-Idopyranosides," *Carbohydrate Research* 445 (2017): 65–74.

31. R. Hevey, A. Morland, and C.-C. Ling, "A Scalable Approach to Obtaining Orthogonally Protected β-D-Idopyranosides," *The Journal of Organic Chemistry* 77 (2012): 6760–6772.

32. P. Zhang, R. Hevey, and C. C. Ling, "Total Synthesis of β-D-Ido-Heptopyranosides Related to Capsular Polysaccharides of *Campylobacter Jejuni* HS:4," *The Journal of. Organic Chemistry* 82 (2017): 9662–9674.

33. S. Homayonia and C.-C. Ling, "Epoxide-Mediated Trans-Thioglycosylation and Application to the Synthesis of Oligosaccharides related to the Capsular Polysaccharides of *C. Jejuni* HS:4," *Chemistry–A European Journal* 30 (2024): e202303753.

34. V. N. Thota and T. L. Lowary, "Synthesis of 6-deoxy-D-ido-Heptopyranose-Containing Fragments of the *Campylobacter Jejuni* Strain CG8486 Capsular Polysaccharide," *Carbohydrate Research* 536 (2024): 109058.

35. T. Li, J. Wang, X. Zhu, et al., "Synthesis of Rare 6-deoxy-D-/L-Heptopyranosyl Fluorides: Assembly of a Hexasaccharide Corresponding to *Campylobacter Jejuni* Strain CG8486 Capsular Polysaccharide," *Journal of the American Chemical Society* 143 (2021): 11171–11179.

36. J. Wang, X. Yang, Z. Huang, et al., "Synthesis of *Campylobacter jejuni* capsular Oligosaccharides and Identification of a Potential O-Antigen Against Campylobacteriosis," *Science Advances* 11 (2025): eadu2318.

37. M. Cloutier, S. Lavoie, and C. Gauthier, "C7 Epimerization of Benzylidene-protected β-D-idopyranosides Brings Structural Insights into Idose Conformational Flexibility," *The Journal of Organic Chemistry* 87 (2022): 12932–12953.

38. R. Das and B. Mukhopadhyay, "The Effect of Neighbouring Group Participation and Possible Long Range Remote Group Participation in O-glycosylation," *Beilstein Journal of Organic Chemistry* 21 (2025): 369–406.

39. A. Ishiwata, K. Tanaka, J. Ao, F. Ding, and Y. Ito, "Recent advances in Stereoselective 1,2-Cis-O-Glycosylations," *Frontiers in Chemistry* 10 (2022): 972429.

40. I. Cumpstey, "Intramolecular Aglycon Delivery," *Carbohydrate Research* 343 (2008): 1553.

41. A. Ishiwata, Y. Lee, and Y. Ito, "Recent Advances in Stereoselective Glycosylation Through Intramolecular Aglycon Delivery," *Organic & Biomolecular Chemistry* 8 (2010): 3596–3608.

42. F. Barresi and O. Hindsgaul, "Synthesis of β-Mannopyranosides by Intramolecular Aglycon Delivery," *Journal of the American Chemical Society* 113 (1991): 9376–9377.

43. Y. Ito, Y. Ohnishi, T. Ogawa, and Y. Nakahara, "Highly Optimized β-Mannosylation Via P-Methoxybenzyl Assisted Intramolecular Aglycon Delivery," *Synlett* 10 (1998): 1102–1104.

44. M. Lergenmüller, T. Nukada, K. Kuramochi, A. Dan, T. Ogawa, and Y. Ito, "On the Stereochemistry of Tethered Intermediate in P-Methoxybenzyl-Assisted β-Mannosylation," *European Journal of Organic Chemistry* 1999 (1999): 1367–1376.

45. Y. Ito, H. Ando, M. Wada, T. Kawai, Y. Ohnish, and Y. Nakahara, "On the mechanism of p-methoxybenzylidene assisted intramolecular aglycon delivery," *Tetrahedron* 57 (2001): 4123–4132.

46. A. Ishiwata, Y. Munemura, and Y. Ito, "NAP Ether Mediated Intramolecular Aglycon Delivery: A Unified Strategy for 1,2-Cis-Glycosylation," *European Journal of Organic Chemistry* 2008 (2008): 4250–4263.

47. Y. Ito and T. Ogawa, "A Novel Approach to the Stereoselective Synthesis of β-Mannosides," *Angewandte Chemie International Edition in English* 33 (1994): 1765–1767.

48. M. Tamigney Kenfack, Y. Blériot, and C. Gauthier, "Intramolecular Aglycon Delivery Enables the Synthesis of 6-Deoxy-β-D-Manno-Heptosides As Fragments of *Burkholderia Pseudomallei* And *Burkholderia Mallei* Capsular Polysaccharide," *The Journal of Organic Chemistry* 79 (2014): 4615–4634.

49. D. M. Ratner, E. R. Swanson, and P. H. Seeberger, "Automated Synthesis of a Protected N-Linked Glycoprotein Core Pentasaccharide," *Organic Letters* 5 (2003): 4717–4720.

50. A. Ishiwata and Y. Ito, "Intramolecular Aglycon Delivery toward 1,2- cis Selective Glycosylation," *Selective Glycosylations: Synthetic Methods and Catalysts* (Ed.: C. S. Bennett, Weinheim: Wiley-VCH) 2017): 79–96.

51. S. Kopitzki and J. Thiem, "Short Synthetic Route to Benzaldehyde-Functionalized Idose and Talose Derivatives by Acetoxonium Ion Rearrangements," *European Journal of Organic Chemistry* 2013 (2013): 4008–4016.

52. P. J. Garegg, T. Iversen, and S. Oscarson, "Monobenzylation of Diols Using Phase-Transfer Catalysis," *Carbohydrate Research* 50 (1976): C12–C14.

53. P. K. Mandal and A. K. Misra, "Synthesis of Oligosaccharides Corresponding to the Polysaccharides of *Lactobacillus* and *Thermophilus* Strains," *Synthesis* 2007 (2007): 2660–2666.

54. L. Jiang and T.-H. Chan, "BoraneBu_2BOTf: A Mild Reagent for the Regioselective Reductive Ring Opening of Benzylidene Acetals in Carbohydrates," *Tetrahedron Letters* 39 (1998): 355–358.

55. Y. Li, X. Yang, Y. Liu, C. Zhu, Y. Yang, and B. Yu, "Gold (I)-Catalyzed Glycosylation with Glycosyl Ortho-Alkynylbenzoates As Donors: General Scope and Application in the Synthesis of a Cyclic Triterpene Saponin," *Chemistry–A European Journal* 16 (2010): 1871–1882.

56. W. A. Bubb, "Nmr Spectroscopy in the Study of Carbohydrates: Characterizing the Structural Complexity," *Concepts in Magnetic Resonance. Part A, Bridging Education and Research.* 19 (2003): 1–19.

57. J. R. Parikh and W. E. Doering, "Sulfur Trioxide in the Oxidation of Alcohols by Dimethyl Sulfoxide," *Journal of the American Chemical Society* 89 (1967): 5505–5507.

58. Y. Tang, J. Li, Y. Zhu, Y. Li, and B. Yu, "Mechanistic Insights into the Gold(I)-Catalyzed Activation of Glycosyl Ortho-Alkynylbenzoates for Glycosidation," *Journal of the American Chemical Society* 135 (2013): 18396–18405.

59. Y. Zhu and B. Yu, "Highly Stereoselective β-Mannopyranosylation Via the 1-α-Glycosyloxy-isochromenylium-4-Gold(I) Intermediates," *Chemistry–A European Journal* 21 (2015): 8771–8780.

60. X. Wang, P. Wang, D. Li, and M. Li, "2,4-Dinitrobenzenesulfonamide-Directed S_N2-Type Displacement Reaction Enables Synthesis of β-D-Glycosaminosides," *Organic Letters.* 21 (2019): 2402–2407.

61. P. Wang, J. Wang, W. Yin, et al., "Direct β-Mannosylation of Primary Alcohol Acceptors: Trisaccharide Iteration Assembly of β-1,6-Oligomannosides Corresponding To Kakelokelose,"*Organic Letters* 24 (2022): 971–976.

62. P. Sun, P. Wang, Y. Zhang, et al., "Construction of β-Mannosidic Bonds Via Gold(I)-Catalyzed Glycosylations with Mannopyranosyl Ortho-Hexynylbenzoates and its Application In Synthesis of Acremomannolipin A," *The Journal of Organic Chemistry* 80 (2015): 4164–4175.

63. I. Pongener, D. A. Pepe, J. J. Ruddy, and E. M. McGarrigle, "Stereoselective β-Mannosylations and β-Rhamnosylations from Glycosyl Hemiacetals Mediated by Lithium Iodide," *Chemical Science* 12 (2021): 10070–10075.

64. J. P. Issa and C. S. Bennett, "A Reagent-Controlled S_n2-Glycosylation for the Direct Synthesis of β-Linked 2-Deoxy-Sugars," *Journal of the American Chemical Society* 136 (2014): 5740–5744.

65. K. Plé, M. Chwalek, and L. Voutquenne-Nazabadioko, "Synthesis of α-Hederin, δ-Hederin, and Related Triterpenoid Saponins," *European Journal of Organic Chemistry* 2004 (2004): 1588–1603.

66. Y. Zhang, H. He, Z. Chen, et al., "Merging Reagent Modulation and Remote Anchimeric Assistance for Glycosylation: Highly Stereoselective Synthesis of α-Glycans Up To A 30-Mer," *Angewandte Chemie International Edition.* 60 (2021): 12597–12606.

Supporting Information

Additional supporting information can be found online in the Supporting Information section. **Supporting Fig. S1:** ^{1}H NMR spectrum ($CDCl_3$, 600 MHz) of ethyl 3-*O*-benzyl-4,6-*O*-benzylidene-1-thio-*α*-D-idopyranoside (7a). **Supporting Fig. S2:** COSY NMR spectrum ($CDCl_3$, 600 MHz) of ethyl 3-*O*-benzyl-4,6-*O*-benzylidene-1-thio-*α*-D-idopyranoside (7a). **Supporting Fig. S3:** $^{13}C\{^{1}H\}$ NMR spectrum ($CDCl_3$, 150 MHz) of ethyl 3-*O*-benzyl-4,6-*O*-benzylidene-1-thio-*α*-D-idopyranoside (7a). **Supporting Fig. S4:** HSQC NMR spectrum ($CDCl_3$, 600 MHz) of ethyl 3-*O*-benzyl-4,6-*O*-benzylidene-1-thio-*α*-D-idopyranoside (7a). **Supporting Fig. S5:** ^{1}H NMR spectrum ($CDCl_3$, 400 MHz) of ethyl 2-*O*-benzyl-4,6-*O*-benzylidene-1-thio-*α*-D-idopyranoside (16). **Supporting Fig. S6:** COSY NMR spectrum ($CDCl_3$, 400 MHz) of ethyl 2-*O*-benzyl-4,6-O-benzylidene-1-thio-*α*-D-idopyranoside (16). **Supporting Fig. S7:** $^{13}C\{^{1}H\}$ NMR spectrum ($CDCl_3$, 100 MHz) of ethyl 2-O-benzyl-4,6-O-benzylidene-1-thio-*α*-D-idopyranoside (16). **Supporting Fig. S8:** HSQC NMR spectrum ($CDCl_3$, 600 MHz) of ethyl 2-*O*-benzyl-4,6-O-benzylidene-1-thio-*α*-D-idopyranoside (16). **Supporting Fig. S9:** ^{1}H NMR spectrum ($CDCl_3$, 600 MHz) of para-methylphenyl 3-*O*-benzyl-4,6-*O*-benzylidene-1-thio-*α*-D idopyranoside (7b). **Supporting Fig. S10:** COSY NMR spectrum ($CDCl_3$, 600 MHz) of para-methylphenyl 3-*O*-benzyl-4,6-*O*-benzylidene-1-thio-*α*-D idopyranoside (7b). **Supporting Fig. S11:** $^{13}C\{^{1}H\}$ NMR spectrum ($CDCl_3$, 150 MHz) of para-methylphenyl 3-*O*-benzyl-4,6-*O*-benzylidene-1-thio-*α*-D idopyranoside (7b). **Supporting Fig. S12:** HSQC NMR spectrum ($CDCl_3$, 600 MHz) of para-methylphenyl 3-*O*-benzyl-4,6-*O*-benzylidene-1-thio-*α*-D idopyranoside (7b). **Supporting Fig. S13:** ^{1}H NMR spectrum ($CDCl_3$, 400 MHz) of ethyl 3-*O*-benzyl-4,6-*O*-benzylidene-2-*O*-para-methoxybenzyl-1-thio-*α*-D idopyranoside (8a). **Supporting Fig. S14:** COSY NMR spectrum ($CDCl_3$, 400 MHz) of ethyl 3-*O*-benzyl-4,6-*O*-benzylidene-2-*O*-para-methoxybenzyl-1-thio α-D-idopyranoside (8a). **Supporting Fig. S15:** $^{13}C\{^{1}H\}$ NMR spectrum ($CDCl_3$, 100 MHz) of ethyl 3-*O*-benzyl-4,6-*O*-benzylidene-2-*O*-para-methoxybenzyl-1 thio-*α*-D-idopyranoside (8a). **Supporting Fig. S16:** HSQC NMR spectrum ($CDCl_3$, 400 MHz) of ethyl 3-*O*-benzyl-4,6-*O*-benzylidene-2-*O*-para-methoxybenzyl-1-thio α-D-idopyranoside (8a). **Supporting Fig. S17:** ^{1}H NMR spectrum ($CDCl_3$, 400 MHz) of para-methylphenyl 3-*O*-benzyl-4,6-*O*-benzylidene-2-*O*-para methoxybenzyl-1-thio-*α*-D-idopyranoside (8b). **Supporting Fig. S18:** COSY NMR spectrum ($CDCl_3$, 400 MHz) of para-methylphenyl 3-*O*-benzyl-4, 6-*O*-benzylidene-2-*O*-para methoxybenzyl-1-thio-α-D-idopyranoside (8b). **Supporting Fig. S19:** $^{13}C\{^{1}H\}$ NMR spectrum ($CDCl_3$, 100 MHz) of para-methylphenyl 3-*O*-benzyl-4,6-*O*-benzylidene-2-*O*-para methoxybenzyl-1-thio-*α*-D-idopyranoside (8b). **Supporting Fig. S20:** HSQC NMR spectrum ($CDCl_3$, 400 MHz) of *para*-methylphenyl 3-*O*-benzyl-4,6-*O*-benzylidene-2-*O*-para-methoxybenzyl-1-thio-*α*-D-idopyranoside (8b). **Supporting Fig. S21:** ^{1}H NMR spectrum ($CDCl_3$, 400 MHz) of ethyl 3,4-di-*O*-benzyl-6-*O*-levulinoyl-2-*O*-para-methoxybenzyl-1-thio-*α*-D idopyranoside (4a). **Supporting Fig. S22:** COSY NMR spectrum ($CDCl_3$, 400 MHz) of ethyl 3,4-di-*O*-benzyl-6-*O*-levulinoyl-2-*O*-*para*-methoxybenzyl-1-thio α-D-idopyranoside (4a). **Supporting Fig. S23:** $^{13}C\{^{1}H\}$ NMR spectrum ($CDCl_3$, 100 MHz) of ethyl 3,4-di-*O*-benzyl-6-*O*-levulinoyl-2-*O*-*para*-methoxybenzyl-1 thio-α-D-idopyranoside (4a). **Supporting Fig. S24:** HSQC NMR spectrum ($CDCl_3$, 400 MHz) of ethyl 3,4-di-O-benzyl-6-*O*-levulinoyl-2-*O*-*para*-methoxybenzyl-1-thio α-D-idopyranoside (4a). **Supporting Fig. S25:**^{1}H NMR spectrum ($CDCl_3$, 400 MHz) of *para*-methylphenyl 3,4-di-*O*-benzyl-2-*O*-*para*-methoxybenzyl-1-thio-α-D idopyranoside (11). **Supporting Fig. S26:** COSY NMR spectrum ($CDCl_3$, 400 MHz) of *para*-methylphenyl 3,4-di-*O*-benzyl-2-*O*-para-methoxybenzyl-1-thio *α*-D-idopyranoside (11). **Supporting Fig. S27:** $^{13}C\{^{1}H\}$ NMR spectrum ($CDCl_3$, 100 MHz) of *para*-methylphenyl 3,4-di-*O*-benzyl-2-*O*-*para*-methoxybenzyl-1-thio *α*-D-idopyranoside (11). **Supporting Fig. S28:** HSQC NMR spectrum ($CDCl_3$, 400 MHz) of *para*-methylphenyl 3,4-di-*O*-benzyl-2-*O*-*para*-methoxybenzyl-1-thio *α*-D-idopyranoside (11). **Supporting Fig. S29:** ^{1}H NMR spectrum ($CDCl_3$, 400 MHz) of *para*-methylphenyl 3,4-di-*O*-benzyl-6-*O*-levulinoyl-2-*O*-*para* methoxybenzyl-1-thio-*α*-D-idopyranoside (4b). **Supporting Fig. S30:** COSY NMR spectrum ($CDCl_3$, 400 MHz) of *para*-methylphenyl 3,4-di-*O*-benzyl-6-*O*-levulinoyl-2-*O*-para methoxybenzyl-1-thio-*α*-D-idopyranoside (4b). **Supporting Fig. S31:**$^{13}C\{^{1}H\}$ NMR spectrum ($CDCl_3$, 100 MHz) of *para*-methylphenyl 3,4-di-*O*-benzyl-6-*O*-levulinoyl-2-*O*-para methoxybenzyl-1-thio-*α*-D-idopyranoside (4b). **Supporting Fig. S32:** HSQC NMR spectrum ($CDCl_3$, 400 MHz) of *para*-methylphenyl 3,4-di-*O*-benzyl-6-*O*-levulinoyl-2-*O*-*para* methoxybenzyl-1-thio-*α*-D-idopyranoside (4b). **Supporting Fig. S33:** ^{1}H NMR spectrum ($CDCl_3$, 400 MHz) of ethyl 3-*O*-benzyl-4,6-*O*-benzylidene-2-*O*-naphthylmethyl-1-thio-*α*-D idopyranoside (9a). **Supporting Fig. S34:** COSY NMR spectrum ($CDCl_3$, 400 MHz) of ethyl 3-*O*-benzyl-4,6-*O*-benzylidene-2-*O*-naphthylmethyl-1-thio-*α*-D idopyranoside (9a). **Supporting Fig. S35:** $^{13}C\{^{1}H\}$ NMR spectrum ($CDCl_3$, 100 MHz) of ethyl 3-*O*-benzyl-4,6-*O*-benzylidene-2-*O*-naphthylmethyl-1-thio-*α*-D idopyranoside (9a). **Supporting Fig. S36:** HSQC NMR spectrum ($CDCl_3$, 400 MHz) of ethyl 3-*O*-benzyl-4,6-*O*-benzylidene-2-*O*-naphthylmethyl-1-thio-*α*-D idopyranoside (9a). **Supporting Fig. S37:** ^{1}H NMR spectrum ($CDCl_3$, 600 MHz) of *para*-methylphenyl 3-*O*-benzyl-4,6-*O*-benzylidene-2-*O*-naphthylmethyl-1 thio-*α*-D-idopyranoside (9b). **Supporting Fig. S38:** COSY NMR spectrum ($CDCl_3$, 600 MHz) of *para*-methylphenyl 3-*O*-benzyl-4,6-*O*-benzylidene-2-*O* naphthylmethyl-1-thio-*α*-D-idopyranoside (9b). **Supporting Fig. S39:** $^{13}C\{^{1}H\}$ NMR spectrum ($CDCl_3$, 150 MHz) of *para*-methylphenyl 3-*O*-benzyl-4,6-*O*-benzylidene-2-*O* naphthylmethyl-1-thio-α-D-idopyranoside (9b). **Supporting Fig. S40:** HSQC NMR spectrum ($CDCl_3$, 600 MHz) of *para*-methylphenyl 3-*O*-benzyl-4,6-*O*-benzylidene-2-*O* naphthylmethyl-1-thio-*α*-D-idopyranoside (9b). **Supporting Fig. S41:** ^{1}H NMR spectrum ($CDCl_3$, 400 MHz) of ethyl 3,4-di-*O*-benzyl-6-*O*-levulinoyl-2-*O*-naphthylmethyl-1-thio-*α*-D idopyranoside (5a). **Supporting Fig. S42:** COSY NMR spectrum ($CDCl_3$, 400 MHz) of ethyl 3,4-di-*O*-benzyl-6-*O*-levulinoyl-2-*O*-naphthylmethyl-1-thio-*α*-D idopyranoside (5a). **Supporting Fig. S43:** $^{13}C\{^{1}H\}$ NMR spectrum ($CDCl_3$, 100 MHz) of ethyl 3,4-di-*O*-benzyl-6-*O*-levulinoyl-2-*O*-naphthylmethyl-1-thio-*α* D-idopyranoside (5a). **Supporting Fig. S44:** HSQC NMR spectrum ($CDCl_3$, 400 MHz) of ethyl 3,4-di-O-benzyl-6-*O*-levulinoyl-2-*O*-naphthylmethyl-1-thio-*α*-D idopyranoside (5a). **Supporting Fig. S45:** ^{1}H NMR spectrum ($CDCl_3$, 600 MHz) of *para*-methylphenyl 3,4-di-*O*-benzyl-6-*O*-levulinoyl-2-*O*-naphthylmethyl 1-thio-*α*-D-idopyranoside (5b). **Supporting Fig. S46.** COSY NMR spectrum ($CDCl_3$, 600 MHz) of *para*-methylphenyl 3,4-di-*O*-benzyl-6-*O*-levulinoyl-2-*O* naphthylmethyl-1-thio-*α*-D-idopyranoside (5b). **Supporting Fig S47.** $^{13}C\{^{1}H\}$ NMR spectrum ($CDCl_3$, 150 MHz) of *para*-methylphenyl 3,4-di-*O*-benzyl-6-*O*-levulinoyl-2-*O* naphthylmethyl-1-thio-*α*-D-idopyranoside (5b). **Supporting Fig. S48:** HSQC NMR spectrum ($CDCl_3$, 600 MHz) of *para*-methylphenyl 3,4-di-*O*-benzyl-6-*O*-levulinoyl-2-*O* naphthylmethyl-1-thio-*α*-D-idopyranoside (5b). **Supporting Fig. S49:** ^{1}H NMR spectrum ($CDCl_3$, 600 MHz) of *para*-methylphenylsulfenyl 3,4-di-*O*-benzyl-6-*O*-levulinoyl-2-*O* naphthylmethyl-*α*-D-idopyranoside (5c). **Supporting Fig. S50:** COSY NMR spectrum ($CDCl_3$, 600 MHz) of *para*-methylphenylsulfenyl 3, 4-di-*O*-benzyl-6-*O*-levulinoyl-2-*O* naphthylmethyl-*α*-D-idopyranoside (5c). **Supporting Fig. S51:** $^{13}C\{^{1}H\}$ NMR spectrum ($CDCl_3$, 150 MHz) of *para*-methylphenylsulfenyl 3,4-di-*O*-benzyl-6-*O*-levulinoyl-2-*O* naphthylmethyl-*α*-D-idopyranoside (5c). **Supporting Fig. S52:** HSQC NMR spectrum ($CDCl_3$, 600 MHz) of *para*-methylphenylsulfenyl 3,4-di-*O*-benzyl-6-*O*-levulinoyl-2-*O* naphthylmethyl-*α*-D-idopyranoside (5c). **Supporting Fig. S53:** ^{1}H NMR spectrum ($CDCl_3$, 600 MHz) of 3, 4-di-*O*-benzyl-6-O-levulinoyl-2-*O*-naphthylmethyl-D-idopyranoside. **Supporting Fig. S54:** COSY NMR spectrum ($CDCl_3$, 600 MHz) of 3,4-di-O-benzyl-6-*O*-levulinoyl-2-*O*-naphthylmethyl-D-idopyranoside. **Supporting Fig. S55:** $^{13}C\{^{1}H\}$ NMR spectrum ($CDCl_3$, 150 MHz) of 3,4-di-*O*-benzyl-6-*O*-levulinoyl-2-*O*-naphthylmethyl-D idopyranoside. **Supporting Fig. S56:** HSQC NMR spectrum ($CDCl_3$, 600 MHz) of 3,4-di-*O*-benzyl-6-*O*-levulinoyl-2-*O*-naphthylmethyl-D-idopyranoside. **Supporting Fig. S57:** undecoupled HSQC NMR

spectrum ($CDCl_3$, 600 MHz) of 3,4-di-*O*-benzyl-6-*O*-levulinoyl-2-*O*-naphthylmethyl-D idopyranoside. **Supporting Fig. S58:** ^1H NMR spectrum ($CDCl_3$, 600 MHz) of 3,4-di-*O*-benzyl-6-*O*-levulinoyl-2-*O*-naphthylmethyl-1-thio-α-D idopyranosyl ortho-hexynylbenzoate (5d). **Supporting Fig. S59:** COSY NMR spectrum ($CDCl_3$, 600 MHz) of 3,4-di-*O*-benzyl-6-*O*-levulinoyl-2-*O*-naphthylmethyl-1-thio-*α*-D idopyranosyl ortho-hexynylbenzoate (5d). **Supporting Fig. S60:** $^{13}C\{^1H\}$ NMR spectrum ($CDCl_3$, 150 MHz) of 3,4-di-*O*-benzyl-6-*O*-levulinoyl-2-*O*-naphthylmethyl-1-thio-*α*-D idopyranosyl ortho-hexynylbenzoate (5d). **Supporting Fig. S61:** HSQC NMR spectrum ($CDCl_3$, 600 MHz) of 3,4-di-*O*-benzyl-6-*O*-levulinoyl-2-*O*-naphthylmethyl-1-thio-*α*-D idopyranosyl ortho-hexynylbenzoate (5d). **Supporting Fig. S62:** undecoupled HSQC NMR spectrum ($CDCl_3$, 600 MHz) of 3,4-di-*O*-benzyl-6-*O*-levulinoyl-2-*O*-naphthylmethyl-1 thio-*α*-D-idopyranosyl ortho-hexynylbenzoate (5d). **Supporting Fig. S63:** ^1H NMR spectrum ($CDCl_3$, 600 MHz) of tert-butyldimethylsilyl 2,4-di-O-benzyl-6-O-levulinoyl-*β*-D-idopyranosyl (1→4)-3,6-di-*O*-benzyl-2-deoxy-2-trichloroacetamido-*β*-D-glucopyranoside (10). **Supporting Fig. S64:** COSY NMR spectrum ($CDCl_3$, 600 MHz) of tert-butyldimethylsilyl 2,4-di-*O*-benzyl-6-*O*-levulinoyl-β-D idopyranosyl-(1→4)-3,6-di-*O*-benzyl-2-deoxy-2-trichloroacetamido-*β*-D-glucopyranoside (10). **Supporting Fig. S65:** $^{13}C\{^1H\}$ NMR spectrum ($CDCl_3$, 150 MHz) of tert-butyldimethylsilyl 2,4-di-O-benzyl-6-*O*-levulinoyl-*β*-D idopyranosyl-(1→4)-3,6-di-*O*-benzyl-2-deoxy-2-trichloroacetamido-*β*-D-glucopyranoside (10). **Supporting Fig. S66:** HSQC NMR spectrum ($CDCl_3$, 600 MHz) of tert-butyldimethylsilyl 2,4-di-*O*-benzyl-6-*O*-levulinoyl-*β*-D idopyranosyl-(1→4)-3,6-di-*O*-benzyl-2-deoxy-2-trichloroacetamido-*β*-D-glucopyranoside (10). **Supporting Fig. S67:** Undecoupled HSQC NMR spectrum ($CDCl_3$, 600 MHz) of tert-butyldimethylsilyl 2,4-di-*O*-benzyl-6-*O*-levulinoyl *β*-D-idopyranosyl-(1→4)-3,6-di-*O*-benzyl-2-deoxy-2-trichloroacetamido-*β*-D-glucopyranoside (10). **Supporting Fig. S68:** ^1H NMR spectrum ($CDCl_3$, 400 MHz) of *para*-methylphenyl 3,4-di-*O*-benzyl-6-deoxy-2-*O*-*para*-methoxybenzyl-1 thio-*α*-D-ido-heptopyranoside (12). **Supporting Fig. S69:** COSY NMR spectrum ($CDCl_3$, 400 MHz) of *para*-methylphenyl 3,4-di-*O*-benzyl-6-deoxy-2-*O*-para methoxybenzyl-1-thio-*α*-D-ido-heptopyranoside (12). **Supporting Fig. S70:** $^{13}C\{^1H\}$ NMR spectrum ($CDCl_3$, 100 MHz) of para-methylphenyl 3,4-di-*O*-benzyl-6-deoxy-2-*O*-para methoxybenzyl-*1*-thio-*α*-D-ido-heptopyranoside (12). **Supporting Fig. S71:** HSQC NMR spectrum ($CDCl_3$, 400 MHz) of *para*-methylphenyl 3,4-di-*O*-benzyl-6-deoxy-2-*O*-para methoxybenzyl-1-thio-*α*-D-ido-heptopyranoside (12). **Supporting Fig. S72:** ^1H NMR spectrum ($CDCl_3$, 400 MHz) of *para*-methylphenyl 3,4-di-*O*-benzyl-6-deoxy-7-*O*-levulinoyl-2-*O*-para methoxybenzyl-1-thio-α-D-ido-heptopyranoside (13). **Supporting Fig. S73:** COSY NMR spectrum ($CDCl_3$, 400 MHz) of *para*-methylphenyl 3,4-di-*O*-benzyl-6-deoxy-7-*O*-levulinoyl-2-*O*-para methoxybenzyl-1-thio-*α*-D-ido-heptopyranoside (13). **Supporting Fig. S74:** $^{13}C\{^1H\}$ NMR spectrum ($CDCl_3$, 100 MHz) of para-methylphenyl 3,4-di-*O*-benzyl-6-deoxy-7-*O*-levulinoyl-2-*O* para-methoxybenzyl-1-thio-*α*-D-ido-heptopyranoside (13). **Supporting Fig. S75:** HSQC NMR spectrum ($CDCl_3$, 400 MHz) of *para*-methylphenyl 3,4-di-*O*-benzyl-6-deoxy-7-*O*-levulinoyl-2-*O*-para methoxybenzyl-1-thio-*α*-D-ido-heptopyranoside (13). **Supporting Fig. S76:** ^1H NMR spectrum ($CDCl_3$, 600 MHz) of *para*-methylphenyl 3-*O*-benzyl-4,6-*O*-benzylidene-2-*O*-tert butyldimethylsilyl-1-thio-*α*-D-idopyranoside (14). **Supporting Fig. S77:** COSY NMR spectrum ($CDCl_3$, 600 MHz) of para-methylphenyl 3-*O*-benzyl-4,6-*O*-benzylidene-2-*O*-tert butyldimethylsilyl-1-thio-*α*-D-idopyranoside (14). **Supporting Fig. S78:** $^{13}C\{^1H\}$ NMR spectrum ($CDCl_3$, 150 MHz) of *para*-methylphenyl 3-*O*-benzyl-4,6-*O*-benzylidene-2-*O*-tert butyldimethylsilyl-1-thio-*α*-D-idopyranoside (14). **Supporting Fig.S79:** HSQC NMR spectrum ($CDCl_3$, 600 MHz) of *para*-methylphenyl 3-*O*-benzyl-4,6-*O*-benzylidene-2-*O*-tert butyldimethylsilyl-1-thio-*α*-D-idopyranoside (14). **Supporting Fig. S80:** ^1H NMR spectrum ($CDCl_3$, 600 MHz) of ethyl 3,4-di-*O*-benzyl-2-*O*-tert-butyldimethylsilyl-6-*O*-levulinoyl-1-thio-α D-idopyranoside (15a). **Supporting Fig. S81:** COSY NMR spectrum ($CDCl_3$, 600 MHz) of ethyl 3,4-di-*O*-benzyl-2-*O*-tert-butyldimethylsilyl-6-*O*-levulinoyl-1 thio-*α*-D-idopyranoside (15a). **Supporting Fig. S82:** $^{13}C\{^1H\}$ NMR spectrum ($CDCl_3$, 150 MHz) of ethyl 3,4-di-*O*-benzyl-2-*O*-tert-butyldimethylsilyl-6-*O*-levulinoyl-1 thio-*α*-D-idopyranoside (15a). **Supporting Fig. S83:** HSQC NMR spectrum ($CDCl_3$, 600 MHz) of ethyl 3,4-di-*O*-benzyl-2-*O*-tert-butyldimethylsilyl-6-*O*-levulinoyl-1 thio-*α*-D-idopyranoside (15a). **Supporting Fig. S84:** ^1H NMR spectrum ($CDCl_3$, 400 MHz) of 3,4-di-*O*-benzyl-2-*O*-tert-butyldimethylsilyl-6-*O*-levulinoyl-D idopyranoside (15b). **Supporting Fig. S85:** COSY NMR spectrum ($CDCl_3$, 400 MHz) of 3,4-di-*O*-benzyl-2-*O*-tert-butyldimethylsilyl-6-*O*-levulinoyl-D idopyranoside (15b). **Supporting Fig. S86:** $^{13}C\{^1H\}$ NMR spectrum ($CDCl_3$, 100 MHz) of 3,4-di-*O*-benzyl-2-*O*-tert-butyldimethylsilyl-6-*O*-levulinoyl-D idopyranoside (15b). **Supporting Fig. S87:** HSQC NMR spectrum ($CDCl_3$, 400 MHz) of 3,4-di-*O*-benzyl-2-*O*-tert-butyldimethylsilyl-6-*O*-levulinoyl-D idopyranoside (15b). **Supporting Fig. S88:** Undecoupled HSQC NMR spectrum ($CDCl_3$, 400 MHz) of 3,4-di-*O*-benzyl-2-*O*-tert-butyldimethylsilyl-6-*O* levulinoyl-D-idopyranoside (15b). **Supporting Fig. S89:** ^1H NMR spectrum ($CDCl_3$, 600 MHz) of 3,4-di-*O*-benzyl-2-*O*-tert-butyldimethylsilyl-6-*O*-levulinoyl-D idopyranosyl ortho-hexynylbenzoate (15c). **Supporting Fig. S90:** COSY NMR spectrum ($CDCl_3$, 600 MHz) of 3,4-di-*O*-benzyl-2-*O*-tert-butyldimethylsilyl-6-*O*-levulinoyl-*D* idopyranosyl ortho-hexynylbenzoate (15c). **Supporting Fig. S91:** $^{13}C\{^1H\}$ NMR spectrum ($CDCl_3$, 150 MHz) of 3,4-di-*O*-benzyl-2-*O*-tert-butyldimethylsilyl-6-*O*-levulinoyl-D idopyranosyl ortho-hexynylbenzoate (15c). **Supporting Fig. S92:** HSQC NMR spectrum ($CDCl_3$, 600 MHz) of 3,4-di-*O*-benzyl-2-*O*-tert-butyldimethylsilyl-6-*O*-levulinoyl-D idopyranosyl ortho-hexynylbenzoate (15c). **Supporting Fig. S93:** undecoupled HSQC NMR spectrum ($CDCl_3$, 600 MHz) of 3,4-di-*O*-benzyl-2-*O*-tert-butyldimethylsilyl-6-*O* levulinoyl-D-idopyranosyl ortho-hexynylbenzoate (15c). **Supporting Fig. S94:** ^1H NMR spectrum ($CDCl_3$, 400 MHz) of N-phenyltrifluoroacetimidate 3,4-di-*O*-benzyl-2-*O*-tert butyldimethylsilyl-6-*O*-levulinoyl-D-idopyranoside (15d). **Supporting Fig. S95:** COSY NMR spectrum ($CDCl_3$, 400 MHz) of N-phenyltrifluoroacetimidate 3,4-di-*O*-benzyl-2-*O*-tert butyldimethylsilyl-6-*O*-levulinoyl-D-idopyranoside (15d). **Supporting Fig. S96:** $^{13}C\{^1H\}$ NMR spectrum ($CDCl_3$, 100 MHz) of N-phenyltrifluoroacetimidate 3,4-di-*O*-benzyl-2-*O*-tert butyldimethylsilyl-6-*O*-levulinoyl-D-idopyranoside (15d). **Supporting Fig. S97:** HSQC NMR spectrum ($CDCl_3$, 400 MHz) of N-phenyltrifluoroacetimidate 3,4-di-*O*-benzyl-2-*O*-tert butyldimethylsilyl-6-*O*-levulinoyl-D-idopyranoside (15d). **Supporting Fig. S98:** Undecoupled HSQC NMR spectrum ($CDCl_3$, 400 MHz) of N-phenyltrifluoroacetimidate 3,4-di-*O*-benzyl-2-*O*-tert butyldimethylsilyl-6-*O*-levulinoyl-D-idopyranoside (15d). **Supporting Fig. S99:** ^1H NMR spectrum ($CDCl_3$, 600 MHz) of tert-butyldimethylsilyl 3,4-di-*O*-benzyl-2-*O*-tert-butyldimethylsilyl-6-*O* levulinoyl-D-idopyranosyl-(1→4)-3,6-di-*O*-benzyl-2-deoxy-2-trichloroacetamido-*β*-D-glucopyranoside (20). **Supporting Fig. S100:** COSY NMR spectrum ($CDCl_3$, 600 MHz) of tert-butyldimethylsilyl 3,4-di-*O*-benzyl-2-*O*-tert-butyldimethylsilyl 6-*O*-levulinoyl-D-idopyranosyl-(1→4)-3,6-di-*O*-benzyl-2-deoxy-2-trichloroacetamido-*β*-D-glucopyranoside (20). **Supporting Fig. S101:** $^{13}C\{^1H\}$ NMR spectrum ($CDCl_3$, 150 MHz) of tert-butyldimethylsilyl 3,4-di-*O*-benzyl-2-*O*-tert-butyldimethylsilyl 6-*O*-levulinoyl-D-idopyranosyl-(1→4)-3,6-di-*O*-benzyl-2-deoxy-2-trichloroacetamido-*β*-D-glucopyranoside (20). **Supporting Fig. S102:** HSQC NMR spectrum ($CDCl_3$, 600 MHz) of tert-butyldimethylsilyl 3,4-di-O-benzyl-2-*O*-tert-butyldimethylsilyl 6-*O*-levulinoyl-D-idopyranosyl-(1→4)-3,6-di-*O*-benzyl-2-deoxy-2-trichloroacetamido-*β*-D-glucopyranoside (20). **Supporting Fig. S103:** Undecoupled HSQC NMR spectrum ($CDCl_3$, 600 MHz) of tert-butyldimethylsilyl 3,4-di-*O*-benzyl-2-*O*-tert butyldimethylsilyl-6-O-levulinoyl-D-idopyranosyl-(1→4)-3,6-di-*O*-benzyl-2-deoxy-2-trichloroacetamido-*β*-D-glucopyranoside (20). **Supporting Fig. S104:** ^1H NMR spectrum ($CDCl_3$, 400 MHz) of ethyl 2-*O*-benzyl-4,6-*O*-benzylidene-3-*O*-tert-butyldimethylsilyl-1-thio *α*-D-idopyranoside (17). **Supporting Fig. S105:** COSY NMR spectrum ($CDCl_3$, 400 MHz) of ethyl 2-*O*-benzyl-4,6-*O*-benzylidene-3-*O*-tert-butyldimethylsilyl-1 thio-*α*-D-idopyranoside (17). **Supporting Fig. S106:** $^{13}C\{^1H\}$ NMR spectrum ($CDCl_3$, 100 MHz) of ethyl 2-*O*-benzyl-4,6-*O*-benzylidene-3-*O*-tert-butyldimethylsilyl-1 thio-*α*-D-idopyranoside (17). **Supporting Fig. S107:** HSQC NMR spectrum ($CDCl_3$, 400 MHz) of ethyl 2-*O*-benzyl-4,6-*O*-benzylidene-3-*O*-tert-butyldimethylsilyl-1 thio-*α*-D-idopyranoside (17). **Supporting Fig. S108:** ^1H NMR spectrum ($CDCl_3$, 400 MHz) of ethyl 2,4-di-*O*-benzyl-3-*O*-tert-butyldimethylsilyl-6-*O*-levulinoyl-1-thio *α*-D-idopyranoside (18). **Supporting Fig. S109:** COSY NMR spectrum ($CDCl_3$, 400 MHz) of

ethyl 2,4-di-*O*-benzyl-3-*O*-tert-butyldimethylsilyl-6-*O*-levulinoyl-1 thio-α-D-idopyranoside (18). **Supporting Fig. S110:** $^{13}C\{^1H\}$ NMR spectrum ($CDCl_3$, 100 MHz) of ethyl 2,4-di-O-benzyl-3-*O*-tert-butyldimethylsilyl-6-*O*-levulinoyl-1 thio-α-D-idopyranoside (18). **Supporting Fig. S111:** HSQC NMR spectrum ($CDCl_3$, 400 MHz) of ethyl 2,4-di-*O*-benzyl-3-*O*-tert-butyldimethylsilyl-6-*O*-levulinoyl-1 thio-α-D-idopyranoside (18). **Supporting Fig. S112:** ^1H NMR spectrum ($CDCl_3$, 500 MHz) of tert-butyldimethylsilyl 2,4-di-*O*-benzyl-3-*O*-tert-butyldimethylsilyl-6-*O* levulinoyl-α-D-idopyranosyl-(1→4)-3,6-di-*O*-benzyl-2-deoxy-2-trichloroacetamido-β-D-glucopyranoside (21). **Supporting Fig. S113:** COSY NMR spectrum ($CDCl_3$, 500 MHz) of tert-butyldimethylsilyl 2,4-di-*O*-benzyl-3-*O*-tert-butyldimethylsilyl 6-*O*-levulinoyl-α-D-idopyranosyl-(1→4)-3,6-di-*O*-benzyl-2-deoxy-2-trichloroacetamido-β-D-glucopyranoside (21). **Supporting Fig. S114:** $^{13}C\{^1H\}$ NMR spectrum ($CDCl_3$, 125 MHz) of tert-butyldimethylsilyl 2,4-di-*O*-benzyl-3-*O*-tert-butyldimethylsilyl 6-*O*-levulinoyl-α-D-idopyranosyl-(1→4)-3,6-di-*O*-benzyl-2-deoxy-2-trichloroacetamido-β-D-glucopyranoside (21). **Supporting Fig. S115:** HSQC NMR spectrum ($CDCl_3$, 500 MHz) of tert-butyldimethylsilyl 2,4-di-*O*-benzyl-3-*O*-tert-butyldimethylsilyl 6-*O*-levulinoyl-α-D-idopyranosyl-(1→4)-3,6-di-*O*-benzyl-2-deoxy-2-trichloroacetamido-β-D-glucopyranoside (21). **Supporting Fig. S116:** Undecoupled HSQC NMR spectrum ($CDCl_3$, 500 MHz) of tert-butyldimethylsilyl 2,4-di-*O*-benzyl-3-*O*-tert butyldimethylsilyl-6-*O*-levulinoyl-α-D-idopyranosyl-(1→4)-3,6-di-*O*-benzyl-2-deoxy-2-trichloroacetamido-β-D-glucopyranoside (21). **Supporting Fig. S117:** ^1H NMR spectrum ($CDCl_3$, 400 MHz) of *para*-methylphenyl 3,4-di-*O*-benzyl-6-deoxy-2,7-di-*O*-para methoxybenzyl-1-thio-α-D-ido-heptopyranoside (22). **Supporting Fig. S118:** COSY NMR spectrum ($CDCl_3$, 400 MHz) of *para*-methylphenyl 3,4-di-*O*-benzyl-6-deoxy-2, 7-di-*O*-para methoxybenzyl-1-thio-α-D-ido-heptopyranoside (22). **Supporting Fig. S119:** $^{13}C\{^1H\}$ NMR spectrum ($CDCl_3$, 100 MHz) of *para*-methylphenyl 3,4-di-*O*-benzyl-6-deoxy-2,7-di-*O*-para methoxybenzyl-1-thio-α-D-ido-heptopyranoside (22). **Supporting Fig. S120:** HSQC NMR spectrum ($CDCl_3$, 400 MHz) of *para*-methylphenyl 3,4-di-*O*-benzyl-6-deoxy-2,7-di-*O*-para methoxybenzyl-1-thio-α-D-ido-heptopyranoside (22). **Supporting Fig. S121:** ^1H NMR spectrum ($CDCl_3$, 400 MHz) of *para*-methylphenyl 7-*O*-acetyl-3,4-di-*O*-benzyl-6-deoxy-2-*O*-*para* methoxybenzyl-1-thio-α-D-ido-heptopyranoside (23). **Supporting Fig. S122:** COSY NMR spectrum ($CDCl_3$, 400 MHz) of *para*-methylphenyl 7-*O*-acetyl-3,4-di-*O*-benzyl-6-deoxy-2-*O*-para methoxybenzyl-1-thio-α-D-ido-heptopyranoside (23). **Supporting Fig. S123:** $^{13}C\{^1H\}$ NMR spectrum ($CDCl_3$, 100 MHz) of para-methylphenyl 7-*O*-acetyl-3,4-di-*O*-benzyl-6-deoxy-2-*O*-para methoxybenzyl-1-thio-α-D-ido-heptopyranoside (23). **Supporting Fig. S124:** HSQC NMR spectrum ($CDCl_3$, 400 MHz) of *para*-methylphenyl 7-*O*-acetyl-3,4-di-*O*-benzyl-6-deoxy-2-*O*-*para* methoxybenzyl-1-thio-α-D-ido-heptopyranoside (23). **Supporting Fig. S125:** ^1H NMR spectrum ($CDCl_3$, 400 MHz) of tert-butyldimethylsilyl 3,4-di-*O*-benzyl-6-deoxy-7-*O*-levulinoyl-2-*O* para-methoxybenzyl-α-D-ido-heptopyranosyl-(1→4)-3,6-di-*O*-benzyl-2-deoxy-2-trichloroacetamido-β-D-glucopyranoside (24α). **Supporting Fig. S126:** COSY NMR spectrum ($CDCl_3$, 400 MHz) of tert-butyldimethylsilyl 3,4-di-*O*-benzyl-6-deoxy-7-O-levulinoyl-2-O *para*-methoxybenzyl-α-D-ido-heptopyranosyl-(1→4)-3,6-di-O-benzyl-2-deoxy-2-trichloroacetamido-β-D-glucopyranoside (24α). **Supporting Fig. S127:** $^{13}C\{^1H\}$ NMR spectrum ($CDCl_3$, 100 MHz) of tert-butyldimethylsilyl 3,4-di-*O*-benzyl-6-deoxy-7-*O*-levulinoyl-2 *O*-para-methoxybenzyl-α-D-ido-heptopyranosyl-(1→4)-3,6-di-*O*-benzyl-2-deoxy-2-trichloroacetamido-β-D-glucopyranoside (24α). **Supporting Fig. S128:** HSQC NMR spectrum ($CDCl_3$, 400 MHz) of tert-butyldimethylsilyl 3,4-di-*O*-benzyl-6-deoxy-7-*O*-levulinoyl-2-*O* *para*-methoxybenzyl-α-D-ido-heptopyranosyl-(1→4)-3,6-di-*O*-benzyl-2-deoxy-2-trichloroacetamido-β-D-glucopyranoside (24α). **Supporting Fig. S129:** Undecoupled HSQC NMR spectrum ($CDCl_3$, 400 MHz) of tert-butyldimethylsilyl 3,4-di-*O*-benzyl-6-deoxy-7-*O* levulinoyl-2-*O*-*para*-methoxybenzyl-α-D-ido-heptopyranosyl-(1→4)-3,6-di-*O*-benzyl-2-deoxy-2-trichloroacetamido-β-D glucopyranoside (24α). **Supporting Fig. S130:** ^1H NMR spectrum ($CDCl_3$, 400 MHz) of tert-butyldimethylsilyl 7-*O*-acetyl-3,4-di-*O*-benzyl-6-deoxy-2-*O*-para methoxybenzyl-α-D-ido-heptopyranosyl-(1→4)-3,6-di-*O*-benzyl-2-deoxy-2-trichloroacetamido-β-D-glucopyranoside (26α). **Supporting Fig. S131:** COSY NMR spectrum ($CDCl_3$, 400 MHz) of tert-butyldimethylsilyl 7-*O*-acetyl-3,4-di-*O*-benzyl-6-deoxy-2-*O*-para methoxybenzyl-α-D-ido-heptopyranosyl-(1→4)-3,6-di-*O*-benzyl-2-deoxy-2-trichloroacetamido-β-D-glucopyranoside (26α). **Supporting Fig. S132:** $^{13}C\{^1H\}$ NMR spectrum ($CDCl_3$, 100 MHz) of tert-butyldimethylsilyl 7-*O*-acetyl-3,4-di-*O*-benzyl-6-deoxy-2-*O* para-methoxybenzyl-α-D-ido-heptopyranosyl-(1→4)-3,6-di-*O*-benzyl-2-deoxy-2-trichloroacetamido-β-D-glucopyranoside (26α). **Supporting Fig. S133:** HSQC NMR spectrum ($CDCl_3$, 400 MHz) of tert-butyldimethylsilyl 7-*O*-acetyl-3,4-di-*O*-benzyl-6-deoxy-2-*O* *para*-methoxybenzyl-α-D-ido-heptopyranosyl-(1→4)-3,6-di-*O*-benzyl-2-deoxy-2-trichloroacetamido-β-D-glucopyranoside (26α). **Supporting Fig. S134:** Undecoupled HSQC NMR spectrum ($CDCl_3$, 400 MHz) of tert-butyldimethylsilyl 7-*O*-acetyl-3,4-di-*O*-benzyl-6 deoxy-2-*O*-*para*-methoxybenzyl-α-D-ido-heptopyranosyl-(1→4)-3,6-di-*O*-benzyl-2-deoxy-2-trichloroacetamido-β-D glucopyranoside (26α). **Supporting Fig. S135:** ^1H NMR spectrum ($CDCl_3$, 400 MHz) of tert-butyldimethylsilyl 7-*O*-acetyl-3,4-di-*O*-benzyl-6-deoxy-2-*O*-para methoxybenzyl-β-D-ido-heptopyranosyl-(1→4)-3,6-di-*O*-benzyl-2-deoxy-2-trichloroacetamido-β-D-glucopyranoside (26β). **Supporting Fig. S136:** COSY NMR spectrum ($CDCl_3$, 100 MHz) of tert-butyldimethylsilyl 7-O-acetyl-3,4-di-*O*-benzyl-6-deoxy-2-*O* para-methoxybenzyl-β-D-ido-heptopyranosyl-(1→4)-3,6-di-*O*-benzyl-2-deoxy-2-trichloroacetamido-β-D-glucopyranoside (26β). **Supporting Fig. S137:** $^{13}C\{^1H\}$ NMR spectrum ($CDCl_3$, 100 MHz) of tert-butyldimethylsilyl 7-*O*-acetyl-3,4-di-*O*-benzyl-6-deoxy-2-*O* *para*-methoxybenzyl-β-D-ido-heptopyranosyl-(1→4)-3,6-di-*O*-benzyl-2-deoxy-2-trichloroacetamido-β-D-glucopyranoside (26β). **Supporting Fig. S138:** HSQC NMR spectrum ($CDCl_3$, 400 MHz) of tert-butyldimethylsilyl 7-*O*-acetyl-3,4-di-*O*-benzyl-6-deoxy-2-*O* *para*-methoxybenzyl-β-D-ido-heptopyranosyl-(1→4)-3,6-di-*O*-benzyl-2-deoxy-2-trichloroacetamido-β-D-glucopyranoside (26β). **Supporting Fig. S139:** Undecoupled HSQC NMR spectrum ($CDCl_3$, 400 MHz) of tert-butyldimethylsilyl 7-*O*-acetyl-3,4-di-*O*-benzyl-6 deoxy-2-*O*-para-methoxybenzyl-β-D-ido-heptopyranosyl-(1→4)-3,6-di-*O*-benzyl-2-deoxy-2-trichloroacetamido-β-D glucopyranoside (26β).